Faculty Publications

6-1-1998

Photochemical production and loss rates of ozone at Sable Island, Nova Scotia during the North Atlantic Regional Experiment (NARE) 1993 summer intensive

Katharine A. Duderstadt
University of New Hampshire, Durham, katharine.duderstadt@unh.edu

M. A. Carroll

S. Sillman

T. Wang

G. M. Albercook

See next page for additional authors

Follow this and additional works at: https://scholars.unh.edu/faculty_pubs

Authors

Katharine A. Duderstadt, M. A. Carroll, S. Sillman, T. Wang, G. M. Albercook, L. Feng, D. D. Parrish, J. S. Holloway, F. C. Fehsenfeld, Donald R. Blake, N. J. Blake, and G. Forbes

Photochemical production and loss rates of ozone at Sable Island, Nova Scotia during the North Atlantic Regional Experiment (NARE) 1993 summer intensive

K. A. Duderstadt,[1] M. A. Carroll,[1,2] S. Sillman,[1] T. Wang, [1,3]
G. M. Albercook,[1] L. Feng,[1] D. D. Parrish,[4] J. S. Holloway, [4]
F. C. Fehsenfeld,[4] D. R. Blake,[5] N. J. Blake,[5] and G. Forbes[6]

Abstract. Three weeks of summertime surface-based chemical and meteorological observations at Sable Island, Nova Scotia during the North Atlantic Regional Experiment (NARE) 1993 summer intensive are used to study instantaneous photochemical production and loss rates of ozone by means of a numerical photochemical model. Results are most sensitive to the averaging scheme of data used to constrain the model and the ambient variability of the measurements. Model simulations driven by a time series of 5 min averaged data, most representative of the chemistry at the site, yield an average net photochemical ozone production of 3.6 ppbv/d. Estimates of net ozone production designed to filter out local sources, by using 1000-1400 LT median values of observations to drive the model and by excluding short-lived hydrocarbons, give values ranging from 1 to 4 ppbv/d. These positive values of net ozone production within the marine boundary layer over Sable Island demonstrate the impact of polluted continental plumes on the background photochemistry of the region during the intensive. The dominant ambient variables controlling photochemical production and loss rates of ozone at the site during the measurement campaign appear to be levels of nitrogen oxides, ozone, nonmethane hydrocarbons, and solar intensity determined by cloud cover. The model partitioning of nitrogen oxides agrees for the most part with measurements, lending credence to calculated photochemical production and loss rates of ozone as well as inferred levels of peroxy radicals not measured at the site. Discrepancies, however, often occur during episodes of intermittent cloud cover, fog, and rain, suggesting the influence of cloud processes on air masses reaching the site.

1. Introduction

Determining the distribution of tropospheric ozone (O_3) and identifying processes responsible for climatological trends in tropospheric ozone levels are priorities in global atmospheric chemistry. By controlling levels of the hydroxyl radical (OH), ozone regulates the oxidation capacity of the troposphere, influencing background levels of trace chemical species [e.g., *Logan et al.,* 1981; *Thompson,* 1992]. Oxidation properties within the atmospheric planetary boundary layer in particular influence the fate of pollutants emitted from the surface as well as the amount of chemical deposition to the biosphere. In addition, ozone within the continental boundary layer directly impacts crops and forests. Indeed, ozone sustained at levels as low as 40 ppbv can significantly reduce crop yields [*U.S. Environmental Protection Agency (EPA),* 1988], of concern because many rural areas of the United States and Europe currently have daytime summertime ozone levels averaging 40-60 ppbv [e.g., *Logan,* 1985; *Logan,* 1989]. Finally, ozone as a greenhouse gas has the potential to perturb the global climate, especially in the upper troposphere where its radiative effects are most significant [e.g., *Intergovernmental Panel on Climate Change (IPCC),* 1990; *Lacis et al.,* 1990].

[1]Department of Atmospheric, Oceanic, and Space Sciences, University of Michigan, Ann Arbor.

[2]Also at Department of Chemistry, University of Michigan, Ann Arbor.

[3]Now at Environmental Engineering Unit, Department of Civil and Structural Engineering, Hong Kong Polytechnic University, Hung Hom, Kowloon, Hong Kong.

[4]Aeronomy Laboratory, National Oceanic and Atmospheric Administration, Boulder, Colorado.

[5]Department of Chemistry, University of California at Irvine.

[6]Atmospheric Environment Service, Sable Island, Nova Scotia, Canada.

There is evidence that background levels of ozone in the northern hemisphere are increasing [e.g., *Volz and Kley*, 1988a; *Marenco and Said*, 1989; *Oltmans and Levy*, 1994]. The initial steps toward identifying the causes as well as the radiative and chemical effects of this trend involve quantifying sources and sinks within the global tropospheric ozone budget. Sources include downward flux from the ozone rich stratosphere, horizontal advection within polluted plumes, and in situ photochemical production. Sinks include deposition at the Earth's surface and in situ photochemical loss.

Early theoretical studies calculate photochemical production and loss rates comparable in magnitude to the dynamical processes of downward transport and surface deposition [e.g., *Fishman et al.*, 1979; *Liu et al.*, 1980]. Within the past decade, researchers have collected chemical and meteorological measurements at a variety of locations throughout the troposphere in order to validate these photochemical theories through numerical photochemical models [e.g., *Chameides et al.*, 1987; *Ridley et al.*, 1992; *Jacob et al.*, 1996]. Figure 1 presents a global map of net photochemical rates of change of ozone integrated over 24 hours (ppbv/day) obtained from the literature for a variety of locations within the planetary boundary layer during late spring, summer, and early fall (based on seasons in the northern hemisphere). Regions over remote oceans such as the eastern North Pacific, equatorial central Pacific, equatorial western Pacific, central North Atlantic, and equatorial Atlantic as well as regions of Alaska not influenced by biomass burning are associated with net photochemical destruction of ozone [e.g., *Liu et al.*, 1983; *Chameides et al.*, 1987; *Carroll et al.*, 1990; *Jacob et al.*, 1992; *Heikes et al.*, 1996; *Davis et al.*, 1996a; *Parrish et al.*, this issue]. Studies in the polluted continental boundary layers over North America and Europe (not shown in Figure 1) and within the continental boundary layer in areas of biomass burning such as over the Amazon forest and over western Alaska (not shown in Figure 1) indicate net ozone production [e.g., *Parrish et al.*, 1986; *Volz et al.*, 1988b; *Jacob and Wofsy*, 1988; *Jacob et al.*, 1992; *Trainer et al.*, 1993; *Kleinman et al.*, 1994; *Carroll and Thompson*, 1995]. These measurements agree for the most part with global model calculations designed to study the relative contributions of transport and photochemistry to the ozone budget [e.g., *Levy et al.*, 1985; *Muller and Brasseur*, 1995; *Atherton et al.*, 1996]. Although it is apparent that human activity is perturbing the photochemistry of the industrialized continental boundary layer, the anthropogenic influence on background photochemistry remains uncertain [e.g., *Hough and Derwent*, 1990; *International Global Atmospheric Chemistry (IGAC)*, 1992].

This paper presents calculations of summertime photochemical ozone production and loss rates for Sable Island, Nova Scotia, an island in the western North Atlantic. This site represents a transitional location between the polluted continent, where one expects to find net photochemical ozone production within the boundary layer, and the clean marine environment, where one expects to find net ozone destruction within the boundary layer. *Parrish et al.* [1993; this issue] present significant evidence of anthropogenic impact from the export of pollution from North America on the chemistry at Sable Island by means of correlations of ozone and carbon monoxide (CO) measured at the site. *Jacob et al.* [1993] discuss continental scale model results generally consistent with these measurements. The addition of measurements of nitrogen oxides and grab samples for hydrocarbon compounds during the North Atlantic Regional Experiment (NARE) 1993 summer intensive provides information for further evaluating this anthropogenic impact on ozone photochemistry at Sable Island. Results indicate that Sable Island is characterized by net ozone production during the intensive, suggesting that this region is close enough to the continent for pollution to significantly modify ozone photochemistry within the marine boundary layer.

2. Measurements and Site

The measurements at Sable Island are part of the NARE 1993 summer intensive. A primary goal of the NARE campaign is to study the impact of anthropogenic emissions from the North American continent on the tropospheric ozone budget over the North Atlantic Ocean [*Fehsenfeld et al.*, 1996a]. The summer intensive hosts a variety of surface-based, airborne, and shipboard measurements described in detail by *Fehsenfeld et al.* [1996b]. The location of Sable Island, one of several surface-based sites spanning the North Atlantic, allows continuous measurements downwind of the polluted North American continent, ideal for assessing the influence of continental plumes on marine boundary layer processes within the regional ozone budget. The Sable Island data set extends from August 14 through September 9 [*Wang et al.*, 1996]. The archived data can be obtained by anonymous ftp to sassarch.sprl.umich.edu in the directory /pub/ARCHIVE/summaries/BL, and *Emmons et al.* [1997] includes a summary of the data within the context of this archive. The photochemical modeling study discussed in this paper focuses on 16 days from this data set, selected based on the availability of concurrent measurements.

A complete description of the Sable Island site and measurement techniques appears in the work of *Wang et al.* [1996]. Briefly, Sable Island is located approximately 180 km off the coast of Nova Scotia (43 55'N; 60 01'W) and 1000 km from the northeastern urban corridor of the United States. The island is a crescent approximately 1 km wide and 40 km long with a maximum elevation of 30 m. Meteorological analyses conclude that the chemical measurements most often characterize the regional marine boundary layer [e.g., *Merrill and Moody*, 1996; *Angevine et al.*, 1996].
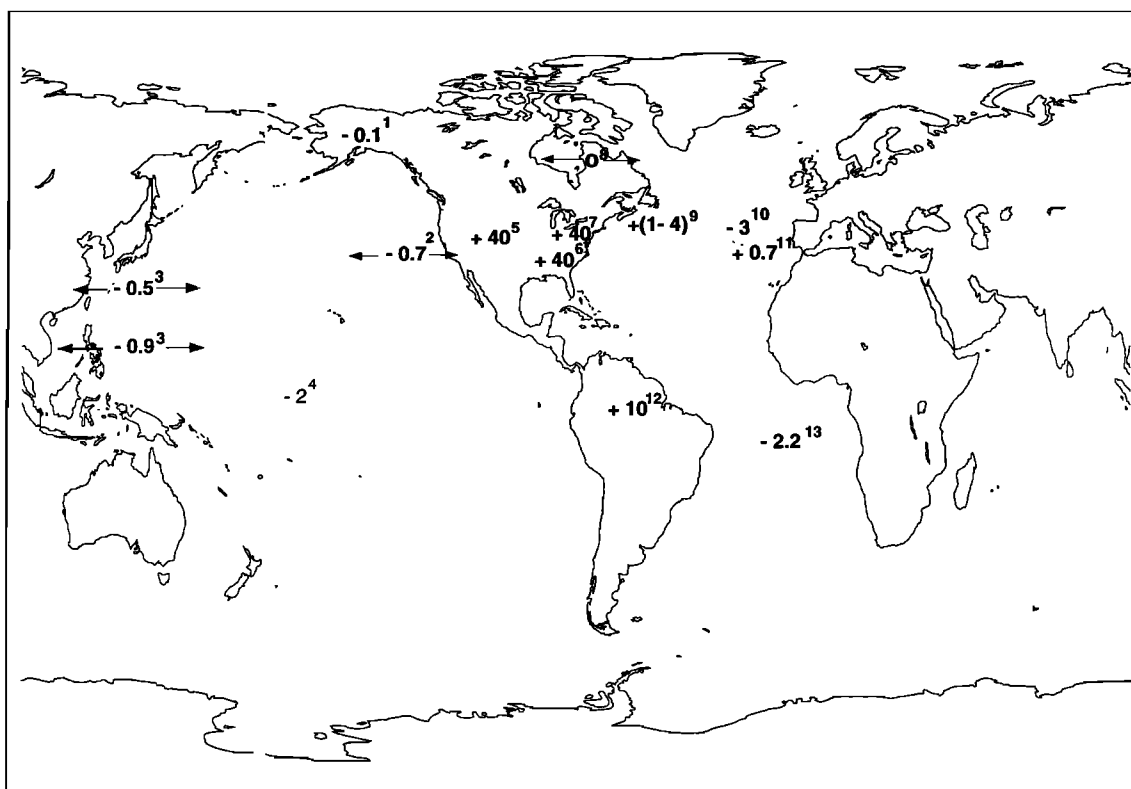
Figure 1. Net photochemical ozone production in the boundary layer determined from measurement and modeling studies around the globe (ppbv/d): (1) *Jacob et al.*, 1992; ABLE-3A; inferred from 24-hour average net photochemical production rates using instantaneous steady state photochemical model calculations based on aircraft measurements within 1 km above the surface over western Alaska during July-August 1988; (2) *Chameides et al.*, 1987; CITE-1; inferred from diurnal average net ozone production determined from both instantaneous steady state as well as diurnal time dependent model calculations for flights from 14°-36°N, 125°-170°W within 0-2 km above the surface during the fall of 1983 [see also Carroll et al., 1990]; CITE-2; presents case studies within the boundary layer; (3) *Davis et al.*, 1996b; PEM-West A; diurnal average rates using a time dependent photochemical model within 0-1 km during September-October, 1991; (4) *Liu et al.*, 1983; Knorr July 1973; from model results for shipboard measurements taken during July and August 1978 from 8°N-8°S, 170°W; (5) referenced in the work of *Carroll and Thompson* [1995]; Niwot Ridge; model results based on surface measurements during June-August 1984; (6) *Kleinman et al.*, 1994; SOS; model results based on surface measurements in rural Georgia during July-August 1991; (7) Referenced in the work of *Carroll and Thompson* [1995]; Scotia, Pennsylvania; June-July 1986; (8) *Mauzerall et al.*, 1996; ABLE-3B; 24 hour average values of net ozone production from an instantaneous steady state model as well as a 1-D time dependent model based on aircraft measurements taken from 45°-63°N, 50°-106°W during July-August 1990; (9) Sable Island; model results presented in this paper based on surface measurements giving net ozone production integrated over 24 hours; August-September 1993 (10) *Parrish et al.*, this issue; Azores; estimated from a modeled ozone decay rate of (0.11 ppbv/d) and an average observed summertime ozone level of 27.8 ppbv; summer 1993; (11) *Noone et al.*, 1996; ASTEX/MAGE; results from a Lagrangian aircraft measurement study during a flight through clean air [see also Carsey et al., 1997]; ASTEX R/V *Malcolm Baldridge*; one-dimensional model calculations indicating a net ozone loss of 8 pptv/d; June-July 1992; (12) *Heikes et al.*, 1996; TRACE-A; model results for the marine boundary layer (0-700 m) from flight observations during September-October 1992 [see also *Jacob et al.*, 1996, Plate 1b]; 13) referenced in the work of *Carroll and Thompson* [1995]; GTE/ABLE-2A; July-August 1985.

The chemical measurements consist of nitric oxide (NO), nitrogen dioxide (NO_2), total reactive nitrogen (NO_y = NO + NO_2 + NO_3 + $2N_2O_5$ + HONO + HO_2NO_2 + PAN + HNO_3 + aerosol nitrate + other organic nitrates), ozone, carbon monoxide, C_2-C_6 hydrocarbons including isoprene, aerosol measurements, and speciated chlorinated compounds. The data set also includes continous measurements of temperature, relative humidity (with which we derive water vapor mixing ratios, H_2O), UV radiation, wind speed, and wind direction along with standard meteorological hourly surface observations and twice daily upper air sondes.

Table 1. Measurement Techniques, Associated Uncertainties, and Ambient Variability Observed at Sable Island during the NARE 1993 Summer Intensive

Parameter	O_3	CO	$NO_x = NO + NO_2$	NMHCs	Noontime J_{NO_2}	Temp
Units	ppbv	ppbv	pptv	ppbC	10^{-3} s^{-1}	K
Technique	UVA [a]	NDIR [b]	P/CL [c]	canister	calculated [d]	
Uncertainty	5% accuracy 1 ppbv precision	10% accuracy 10 ppbv precision	35%	5% accuracy 5% precision	±5% (clear skies) ±20% (overcast)	±1 K
Minimum	15	50	8	1.2	3.4×10^{-3}	286
Lower 95%	18	77	19	2.7	3.6×10^{-3}	288
Lower 67%	22	97	44	3.5	4.5×10^{-3}	289
Median	28	110	97	5.1	8.0×10^{-3}	291
Mean	30	115	190	6.8	6.8×10^{-3}	291
Upper 67%	35	136	266	8.3	8.4×10^{-3}	292
Upper 95%	51	173	881	17.9	8.7×10^{-3}	294
Maximum	88	260	6953	48.3	8.8×10^{-3}	296
n	5343	5359	3602	81	16	4935

[a] Ultraviolet absorption [Parrish et al., 1993].
[b] Nondispersive infrared [Parrish et al., 1994].
[c] Photolysis of NO_2 followed by chemiluminescense detection of NO by reaction with O_3 [Wang et al., 1996].
[d] Calculated from Eppley UV measurements [Madronich, 1987b].

The chemical measurements within the Sable Island data set have been filtered using the criteria for NO, NO_2, and NO_y described by Wang et al. [1996], removing data associated with local pollution from the island generator and passing vehicles as well as data collected when wind speeds are less than 1 m/s. For this study we use 5 min averages of all chemical and meteorological measurements except for nonmethane hydrocarbons, which are available from grab samples four to six times daily.
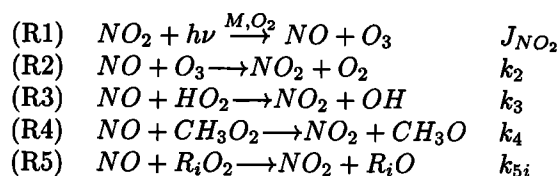
Table 1 lists the measurement techniques and the associated uncertainties for O_3, nitrogen oxides (NO_x = NO + NO_2), CO, NMHCs, and J_{NO_2} (derived from Eppley radiometer measurements). This table also presents statistics associated with the ambient variability of these measurements during the entire campaign. Elevated levels of NO_x, O_3, and CO occur during a multiday pollution episode centered around August 28. The data set exhibits more frequent variability in NO_x, presumed to originate from fresh sources such as ship traffic and an oil production platform 40 km to the southwest [Wang et al., 1996].

3. Photochemical Theory

Generally, the large photochemical production and loss rates of ozone calculated throughout the troposphere attain near balance, resulting in small net rates of change. These net photochemical effects are difficult to discern from field measurements. As a consequence, analytical theory and numerical photochemical models are usually required to assess ozone photochemistry.

Ozone is produced through the oxidation of volatile organic compounds (e.g., CH_4, CO, and NMHCs) in the presence of odd hydrogen (HO_x = OH + HO_2), NO_x,

and sunlight. Detailed descriptions of the gas-phase photochemical reactions of ozone photochemistry appear throughout the literature [e.g., Lurmann et al., 1986; Liu et al., 1987; Trainer et al., 1987; Carter, 1990]. These theories rely on the assumption that the following reactions approximate photochemical steady state:

(R1) $NO_2 + h\nu \xrightarrow{M,O_2} NO + O_3$ J_{NO_2}
(R2) $NO + O_3 \longrightarrow NO_2 + O_2$ k_2
(R3) $NO + HO_2 \longrightarrow NO_2 + OH$ k_3
(R4) $NO + CH_3O_2 \longrightarrow NO_2 + CH_3O$ k_4
(R5) $NO + R_iO_2 \longrightarrow NO_2 + R_iO$ k_{5i}

where HO_2 refers to hydrogen peroxy radicals, CH_3O_2 refers to methyl peroxy radicals, and R_iO_2 refers to organic peroxy radicals other than CH_3O_2. Peroxy radicals result from the oxidation of CO, CH_4, and NMHCs. Measurement and modeling studies in many locations show evidence of peroxy radicals as additional NO to NO_2 oxidants leading to (R3)-(R5) [e.g., Parrish et al., 1986; Chamedies et al., 1990; Ridley et al., 1992]. In this study, we separate CH_3O_2 from the other organic peroxy radicals in an effort to more adequately address the role of nonmethane hydrocarbons in ozone photochemistry at Sable Island.

The assumption of photochemical steady state implies that the reaction rates (R1)-(R5) are sufficiently fast as to allow the system to reach chemical equilibrium within the timescale of fluctuations in solar intensity. Although a detailed examination of the photochemical steady state assumption is not included in this study, it is important to recognize that scattered cloud cover, causing rapid changes in solar flux, could invalidate this assumption [Cantrell et al., 1993].

The oxidation of NO to NO_2 through reactions (R1)-(R5) yields the following steady state NO/NO_2 ratio:

$$\frac{[NO]}{[NO_2]} = \frac{J_{NO_2}}{k_2[O_3] + k_3[HO_2] + k_4[CH_3O_2] + \Sigma k_{5i}[R_iO_2]} \quad (1)$$
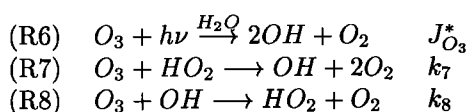
and ozone production rate:

$$
\begin{aligned}
P(O_3) &= k_3[NO][HO_2] + k_4[NO][CH_3O_2] \\
&\quad + \Sigma k_{5i}[NO][R_iO_2] \\
&= [NO_2]J_{NO_2} - [NO][O_3]k_2 \quad (2)
\end{aligned}
$$

Equation (3) and the assumption $k_3 \approx k_4 \approx k_{5i}$ allow the following analytical expression for total peroxy radicals:

$$
\begin{aligned}
\sum RO_2 &= [HO_2] + [CH_3O_2] + \Sigma[R_iO_2] \\
&\approx \frac{J_{NO_2}[NO_2]}{[NO][k_3]} - [O_3]\frac{k_2}{k_3} \quad (3)
\end{aligned}
$$

In this study we use equations (2) and (3) to determine photochemical ozone production and total peroxy radical levels for the Sable Island data set using chemical and meteorological parameters obtained through measurements. We then compare these values to results from a numerical photochemical model involving a more explicit chemical mechanism which we describe in the next section.

Ozone destruction occurs primarily by means of the following reactions:

(R6) $O_3 + h\nu \xrightarrow{H_2O} 2OH + O_2$ $J^*_{O_3}$
(R7) $O_3 + HO_2 \longrightarrow OH + 2O_2$ k_7
(R8) $O_3 + OH \longrightarrow HO_2 + O_2$ k_8

with minor losses through the ozonolysis of alkenes. $J^*_{O_3}$ is an effective photodissociation rate referring to the net reaction of O_3 photolysis followed by the reaction of $O(^1D)$ with water vapor [e.g., Ridley et al., 1992]. These reactions yield an expression for ozone loss:

$$L(O_3) = J^*_{O_3}[O_3] + k_7[O_3][HO_2] + k_8[O_3][OH] \quad (4)$$

As measurements of $J^*_{O_3}$, HO_2, and OH were not made at the site, this study relies on numerical photochemical model calculations to estimate ozone loss rates.

4. Photochemical Model

The photochemical model used in this study is described in detail by Sillman et al. [1990a; 1993]. Briefly, the model is based on the gas-phase chemical mechanism from Lurmann et al. [1986], comprised of reactions involving O_3, NO_x, HO_x, and C_2-C_7 hydrocarbons (note that the self reaction of HO_2 to form H_2O_2 takes into account the dependence on water vapor, consistent with Stockwell [1995]). Modifications from Ja-

cob and Wofsy [1988] address low NO_x concentrations characteristic of the remote environment. The chemical mechanism uses rate constants from DeMore et al. [1992], adjusting these rates as functions of temperature, pressure, and humidity. Photolysis rates for NO_2 are available from calculations based on Eppley radiometer measurements [Madronich, 1987b]. However, photolysis rates for other species, especially J_{O_3}, cannot be determined from either Eppley radiometer measurements or from an assumed ratio to the measured J_{NO_2}. These rates are calculated using the radiative transfer model of Madronich [1987a] and take into account latitude and time of day. Cloud optical depth in the radiative transfer calculation is inferred by choosing values that generate J_{NO_2} equal to measured values. The calculation assumes that total ozone column density is 320 Dobson units (DU), characteristic of the site during the month of August [Fishman et al., 1990]. Concurrent measurements of total column ozone would provide more representative results, but this information was not available at the time of this analysis.

The Sillman et al. [1993] model is part of the Intergovernmental Panel on Climate Change Photochemical Model Intercomparison [Olson et al., 1997]. This study demonstrates a consistency in net O_3 production among all the models for simulations of a marine environment, with a variation about the mean of 10%.

The simulations are set up as time dependent box model photochemical calculations. Longer-lived species (O_3, total NO_x, CO, NMHCs), presumed to be influenced more by meteorology than by diurnal photochemistry, are used to initialize and constrain the model simulations according to the diurnal time series observed at Sable Island during the day being represented (with simulations done separately for each of the 16 days). Intermediate species (e.g., aldehydes and ketones) are allowed to reach steady state by spinning up the model through five diurnal cycles before recording the results. Levels of shorter-lived species (e.g., NO, NO_2, OH, and peroxy radicals) and instantaneous production and loss rates comprise the output.

Species that are long-lived but are not included in the suite of measurements at Sable Island are prescribed using values obtained from the literature: methane equal to 1.7 ppmv [Wild et al., 1996] and molecular hydrogen equal to 0.58 ppmv [Seinfeld, 1986]. Following the nomenclature of Lurmann et al. [1986], C_4 - C_5 alkanes determined from grab samples at the site (n-butane, i-butane, n-pentane, and i-pentane) are lumped in the model mechanism under alk4. Similarly, hexane (C_6) is included in the mechanism under the lumped alk7. Hydrocarbons not determined at the site, and consequently not included in the model runs, include xylene and butene. Primary sources of butene are anthropogenic. The short lifetimes of cis- and trans-2-butene, approximately 30 min [Finlayson-Pitts and Pitts, 1986], suggest that transport from the continent over the ocean will not significantly contribute to levels

observed at the site. Local sources of butene and xylene, however, might be present from emissions on the island, passing ships, or the oil platform to the southwest.

Questions remain concerning the validity of allowing the intermediate species to reach steady state through the five diurnal cycle spin-up time. For our model simulations, changes in concentrations of selected intermediate species during the final day of model spin-up time are as follows: formaldehyde (2%), acetaldehyde (2%), higher aldehydes (6%), hydrogen peroxide (3%), acetone (22%), and methyl ethyl ketone (15%). Because acetone and methyl ethyl ketone take much longer to reach steady state, initial concentrations of these species are set at nonzero at the beginning of the simulation. Allowing intermediate species to reach steady state is valid only if the photochemical age of the air mass from the time of emissions is longer than the time it takes a given species to reach steady state in the model simulation. Back trajectories indicate transport times ranging from 1-5 days from continental source regions with the additional possibility of accumulation from prior emissions over the continent [*Merrill and Moody*, 1996] suggesting that a 5 day spin-up time is adequate for representing much of the campaign. We furthermore assume the same diurnal cloud pattern for the 5 day spin-up time based on J_{NO_2} values calculated from Eppley radiometer measurements. In reality, air masses most likely traveled under different cloud conditions before reaching the site. Running the model with 5 days of spin-up time under clear-sky conditions before encountering the observed cloud conditions gives values of net

ozone production greater on average by 4%, with a maximum increase of 20% occurring on the overcast day of September 5.

We explore several different averaging schemes for using the measurements of longer-lived species to drive the model. The first scheme (hereafter referred to as FIVEMIN) updates concentrations of O_3, total NO_x, CO, and NMHCs as well as levels of relative humidity, temperature, and solar intensity at each 5 min time step using the time series of 5 min averages of the observations. We interpolate values linearly when concurrent measurements are not available. The second scheme (hereafter referred to as MEDIAN) relies on constant values of O_3, total NO_x, CO, NMHCs, and relative humidity to constrain the model at the beginning of each time step using median values of the measurements made during peak photochemical activity, 1000-1400 local time [local solar time equal to Atlantic standard time (AST)]. In the second set of simulations, temperature is allowed to vary smoothly throughout the diurnal simulation using parameters derived from a sinusoidal fit to the measurements. Similarly, photolysis rates are allowed to vary diurnally, based on the photolysis calculation described above, with a constant cloud optical depth determined from a second-degree polynomial fit to measured J_{NO_2} from 1000 to 1400. A third scheme (hereafter referred to as MEAN) is similar to the second but uses mean values of measurements during the 1000-1400 LT time window to constrain the model. Median, mean, and standard deviations for the 1000-1400 LT time window are presented in Table 2. Periods of

Table 2a. The 1000-1400 LT Mean Values of Temperature, Noontime J_{NO_2}, and Periods of Precipitation and Cloud Cover from the Sable Island Data Set

Date	Temperature, K	Precipitation, LT	Fog, LT	Noontime J_{NO_2}, $10^{-3} s^{-1}$
Aug. 19	290.3	10-11		4.48
Aug. 21	290.1	8-10, 13-15	4-15	3.60
Aug. 22	289.6			8.77
Aug. 23	289.1			8.24
Aug. 24	289.5			8.42
Aug. 25	290.7	15-17		8.38
Aug. 26	291.4		4-9	8.32
Aug. 27	291.3			8.24
Aug. 28	292.0		all day	5.15
Aug. 29	291.0			7.13
Aug. 30	290.6			8.67
Aug. 31	289.5			8.04
Sept. 1	291.8	15-16	15-19	4.02
Sept. 3	290.1	6-8, 13	6-19	5.83
Sept. 4	293.2		0-8, 15-23	7.94
Sept. 5	291.5	13-14, 17-19	all day	3.38
Mean ($\pm\sigma$)	290.7 (1.1)			6.79 (2.0)
Median	290.7			7.99
Maximum	293.2			8.77
Minimum	289.1			3.38
n	16			16

Table 2b. The 1000-1400 LT Mean Values, Median Values, and Standard Deviations (in Parentheses) of H_2O and O_3 from the Sable Island Data Set

Date	H_2O, parts per thousand			O_3, ppbv		
	Mean(σ)	Median	n	Mean(σ)	Median	n
Aug. 19	16.8 (0.1)	16.9	48	29 (1)	31	121[a]
Aug. 21	18.7 (0.2)	18.6	48	24 (1)	24	25
Aug. 22	15.2 (0.5)	15.4	34	20 (1)	20	38
Aug. 23	14.9 (0.6)	15.1	48	23 (1)	22	40
Aug. 24	16.0 (0.4)	16.1	48	30 (4)	29	37
Aug. 25	17.7 (0.2)	17.8	48	40 (1)	40	35
Aug. 26	18.8 (0.1)	18.9	48	31 (3)	36	38
Aug. 27	15.7 (0.4)	15.8	48	35 (2)	34	39
Aug. 28	19.7 (0.7)	20.0	48	73 (8)	72	37
Aug. 29	18.5 (0.2)	18.5	48	42 (2)	43	35
Aug. 30	14.6 (1.5)	14.8	48	31 (1)	31	39
Aug. 31	10.2 (0.1)	10.2	48	29 (4)	28	39
Sept. 1	19.4 (0.4)	19.9	48	36 (1)	36	25
Sept. 3	18.4 (0.4)	18.5	48	27 (1)	27	35
Sept. 4	22.1 (0.3)	22.1	48	32 (4)	34	39
Sept. 5	20.7 (0.5)	20.7	48	20 (1)	19	35
Mean ($\pm\sigma$)	17.4 (2.9)	17.5 (2.9)		33 (13)	33 (12)	
Median	18.1	18.2		31	31	
Maximum	22.1	22.1		73	72	
Minimum	2.9	10.2		20	19	
n	16	16		16	16	

[a]Statistics on August 19 are based on measurements taken over the entire day because data are not available from 1000-1400 LT.

Table 2c. The 1000-1400 LT Mean Values, Median Values, and Standard Deviations (in Parentheses) of NO_x and CO from the Sable Island Data Set

Date	NO_x, pptv			CO, ppbv		
	Mean(σ)	Median	n	Mean(σ)	Median	n
Aug. 19	60 (70)	38	122[a]	99 (4)	99	122[a]
Aug. 21	1178 (1373)	620	38	96 (3)	95	26
Aug. 22	86 (34)	75	38	101 (5)	100	38
Aug. 23	57 (48)	34	40	102 (4)	103	40
Aug. 24	90 (11)	93	37	112 (8)	110	37
Aug. 25	76 (19)	69	35	126 (5)	127	35
Aug. 26	271 (116)	232	38	161 (7)	164	38
Aug. 27	136 (20)	145	39	118 (4)	119	39
Aug. 28	46 (11)	44	37	223 (21)	221	37
Aug. 29	131 (34)	126	35	163 (7)	165	35
Aug. 30	90 (17)	88	39	114 (5)	113	39
Aug. 31	118 (17)	40	41	103 (6)	105	39
Sept. 1	69 (38)	58	25	118 (5)	118	25
Sept. 3	38 (7)	38	35	112 (5)	112	35
Sept. 4	70 (58)	44	39	116 (9)	117	39
Sept. 5	391 (186)	434	35	80 (5)	80	35
Mean ($\pm\sigma$)	182 (281)	136 (160)		122 (35)	122 (35)	
Median	88	72		113	113	
Maximum	1178	620		223	221	
Minimum	38	34		80	80	
n	16	16		16	16	

[a]Statistics on August 19 are based on measurements taken over the entire day because data are not available from 1000-1400 LT.

Table 2d. The 1000-1400 LT Mean Values, Median Values, and Standard Deviations (in Parentheses) of Alkanes from the Sable Island Data Set

Date	Ethane, pptv[a]		Propane, pptv		Alk4[b], pptv		Alk7[c], pptv	
	Mean(σ)	Median	Mean(σ)	Median	Mean(σ)	Median	Mean(σ)	Median
Aug. 19	870 (18)	871	62 (9)	60	160 (3)	161	13 (0)	13
Aug. 21	863 (8)	865	265 (32)	271	574 (35)	577	19 (1)	19
Aug. 22	865 (5)	864	156 (4)	156	164 (4)	162	10 (0)	10
Aug. 23	816 (1)	816	83 (5)	83	155 (2)	155	11 (1)	11
Aug. 24	899 (26)	901	307 (67)	323	670 (172)	716	25 (4)	26
Aug. 25	833 (15)	828	122 (25)	104	179 (12)	178	13 (1)	13
Aug. 26	1474 (47)	1480	791 (12)	793	1210 (183)	1220	40 (6)	39
Aug. 27	953 (15)	953	130 (5)	128	210 (12)	212	6 (1)	6
Aug. 28	1396 (97)	1400	394 (81)	388	335 (87)	331	6 (1)	6
Aug. 29	1069 (52)	1050	224 (60)	201	316 (68)	290	8 (3)	6
Aug. 30	971 (99)	906	141 (35)	115	177 (114)	168	8 (0)	8
Aug. 31	852 (22)	856	85 (13)	93	132 (12)	141	7 (1)	7
Sept. 1	915 (25)	928	156 (7)	156	191 (17)	191	5 (0)	5
Sept. 3	720 (26)	938	100 (33)	123	215 (41)	252	10 (0)	11
Sept. 4	896 (85)	929	176 (17)	185	183 (17)	177	5 (2)	4
Sept. 5	614 (80)	617	455 (168)	461	1200 (440)	1220	36 (10)	36
Mean ($\pm\sigma$)	938 (219)	950 (210)	228 (188)	228 (190)	379 (357)	384 (360)	14 (11)	14 (11)
Median	883	904	156	156	201	202	10	11
Maximum	1474	1480	791	793	1210	1220	40	39
Minimum	614	617	62	60	132	141	5	4
n	16	16	16	16	16	16	16	16

[a]Values of NMHCs are based on 5 min linear interpolations from grab samples.
[b]Denotes n-butane, i-butane, n-pentane, and i-pentane
[c]Hexane

Table 2e. The 1000-1400 LT Mean Values, Median Values, and Standard Deviations (in Parentheses) of Alkenes from the Sable Island Data Set

Date	Ethene, pptv		Propene, pptv		Isoprene, pptv	
	Mean(σ)	Median	Mean(σ)	Median	Mean(σ)	Median
Aug. 19	58 (29)	52	56 (25)	51	13 (0)	13
Aug. 21	59 (1)	59	63 (2)	63	17 (1)	17
Aug. 22	71 (5)	70	60 (5)	59	46 (4)	47
Aug. 23	43 (1)	43	41 (2)	41	24 (2)	24
Aug. 24	32 (2)	31	51 (2)	53	70 (15)	74
Aug. 25	80 (4)	83	79 (6)	80	63 (6)	64
Aug. 26	280 (43)	281	118 (19)	119	43 (4)	43
Aug. 27	38 (7)	34	29 (4)	30	123 (14)	132
Aug. 28	68 (30)	69	54 (25)	54	111 (30)	113
Aug. 29	145 (17)	136	114 (16)	105	21 (18)	12
Aug. 30	92 (45)	61	89 (50)	52	92 (5)	95
Aug. 31	49 (20)	47	50 (10)	50	45 (2)	46
Sept. 1	121 (37)	143	84 (24)	98	116 (31)	129
Sept. 3	42 (13)	50	41 (20)	56	65 (46)	26
Sept. 4	33 (11)	25	27 (12)	19	76 (17)	79
Sept. 5	57 (2)	57	40 (5)	40	81 (13)	81
Mean ($\pm\sigma$)	79 (62)	78 (64)	62 (28)	61 (27)	63 (36)	62 (40)
Median	59	58	55	54	64	56
Maximum	280	281	118	119	123	132
Minimum	32	25	27	19	13	12
n	16	16	16	16	16	16

Table 2f. The 1000-1400 LT Mean Values, Median Values, and Standard Deviations (in Parentheses) of Aromatics from the Sable Island Data Set

Date	Acetylene, pptv[a]		Benzene, pptv		Toluene, pptv	
	Mean(σ)	Median	Mean(σ)	Median	Mean(σ)	Median
Aug. 19	177(28)	171	68 (5)	67	24 (4)	23
Aug. 21	150 (1)	150	58 (6)	56	67 (11)	62
Aug. 22	146 (3)	146	74 (1)	74	116 (7)	118
Aug. 23	134 (1)	134	58 (1)	58	115 (12)	116
Aug. 24	150 (4)	153	69 (5)	66	68 (15)	60
Aug. 25	224 (12)	231	110 (12)	102	54 (0)	54
Aug. 26	323 (20)	324	191 (12)	191	160 (8)	160
Aug. 27	144 (8)	140	106 (5)	103	83 (4)	82
Aug. 28	389 (73)	385	179 (8)	182	118 (6)	115
Aug. 29	284 (44)	281	162 (53)	142	168 (8)	167
Aug. 30	149 (18)	137	101 (2)	100	97 (1)	98
Aug. 31	112 (9)	114	117 (16)	122	97 (11)	101
Sept. 1	266 (62)	302	122 (65)	95	84 (0)	84
Sept. 3	132 (2)	131	96 (29)	112	115 (44)	97
Sept. 4	132 (10	138	98 (26)	80	63 (3)	64
Sept. 5	79 (2)	79	208 (63)	211	56 (2)	57
Mean ($\pm\sigma$)	187 (86)	189 (88)	114 (48)	110 (48)	93 (39)	91 (39)
Median	150	148	104	101	91	91
Maximum	389	385	208	211	168	167
Minimum	79	79	58	56	24	23
n	16	16	16	16	16	16

[a] Acetylene is not included in the model simulations.

fog and rain recorded by surface observations are also indicated in Table 2 (in LT) for later reference.

The FIVEMIN simulations reflect the measured variability of chemical and meteorological parameters such as NO_x and solar intensity [*Wang et al.*, 1996] and most accurately represent the photochemistry at the site. The MEDIAN simulations are more likely to reflect regional background conditions by considering the chemistry during peak photochemical activity and by filtering out peaks in NO_x and NMHCs presumed to originate from local sources. We choose median values to be representative of regional photochemistry as opposed to mean values because the distribution of NO_x measurements is skewed by short-lived peaks [*Wang et al.*, 1996]. However, we include the MEAN simulations for completeness.

We evaluate the model by comparing model-calculated NO/NO_2 ratios with NO/NO_2 ratios determined from the measurements of NO and NO_2 as well as model-calculated ΣRO_2 with values determined from measurements using equation (3). We consider observed 5 min averages as well as model calculations at 5 min intervals from 0800-1600 LT in order to avoid potential complications associated with sunrise and sunset. Figure 2 shows the correlation of NO/NO_2 ratios calculated by the FIVEMIN simulations and NO/NO_2 ratios made up of 5 min averaged NO and NO_2 measurements. Figure 3 shows a similar correlation for peroxy radical mixing ratios. Overlaid onto these figures are binned averages, each representing 20% (by number of points) of the cal-
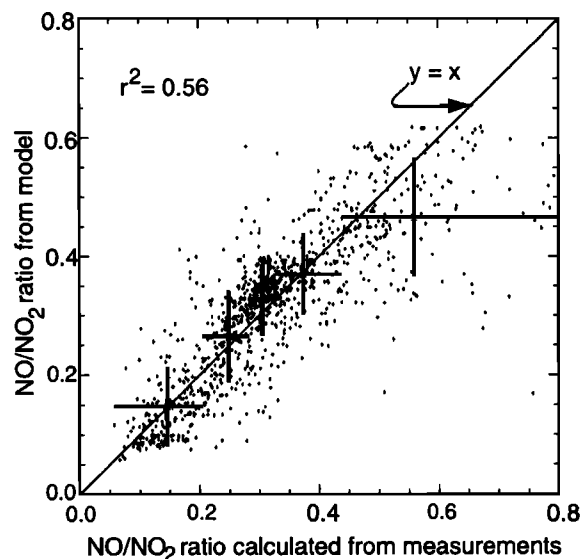
Figure 2. Correlation of daytime (0800-1600 LT) NO/NO_2 ratios from model calculations using FIVEMIN simulations and NO/NO_2 ratios from measurements. The total number of points is 1060, 1% of which are not shown because the calculations from the measurements are greater than 0.8. Averages of model and measurement values based on 20% of the results (by number) are overlaid onto the figure. Vertical bars represent standard deviations of the model results. Horizontal bars represent the range based on calculations from measurements for each average. A line with a slope equal to one also appears on the figure. Two-sided linear regression (line of organic correlation [see *Hirsh and Gilroy*, 1984]) gives y = 0.72 x + 0.084.
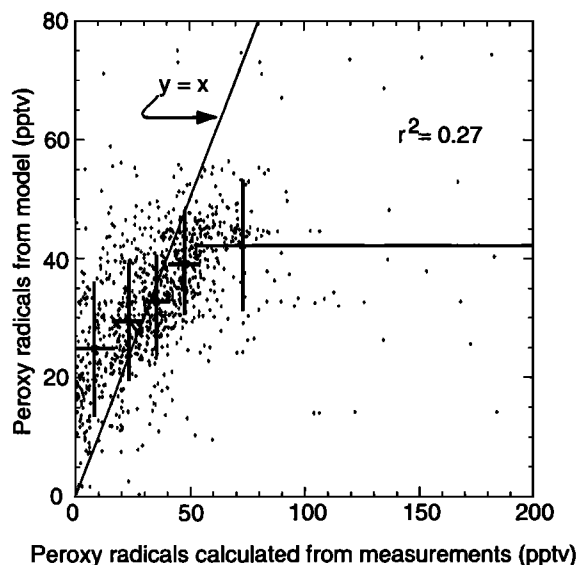
Figure 3. Correlation of daytime (0800-1600 LT) peroxy radical mixing ratios from model calculations using 5 min input values and peroxy radical mixing ratios calculated from measurements using equation (3). Symbols are the same as in Figure 2. Two-sided linear regression gives $y = 0.25\,x + 24$.

culations. The vertical error bars refer to standard deviations of the model output. The horizontal error bars depict the range of the values from measurements over which each average is determined.

The correlation between calculations from the model and measurements for the NO/NO_2 ratios is positive, with a square of the correlation coefficient $r^2 = 0.56$. The binned averages show a significant trend, with the lowest 80% of the points falling close to the line with slope equal to 1.0. The model, however, does not reproduce the few high NO/NO_2 ratios (greater than 0.6) determined from the measurements. The high NO/NO_2 ratios determined from measurements may result from nonsimultaneous measurements of NO and NO_2 [*Wang et al.*, 1996] combined with rapid fluctuations in solar intensity caused by cloud cover.

The comparison of model peroxy radical levels and levels derived from measurements via equation (3) (Figure 3) shows agreement in terms of the average magnitude of ΣRO_2 (0800-1600 LT averages: 34 pptv ΣRO_2 from the model and 38 pptv ΣRO_2 calculated from measurements). Furthermore, model calculations of ΣRO_2 using the model output of NO, NO_2, k_2, k_3, J_{NO_2}, and O_3 along with equation (3) agree well with model ΣRO_2 determined from the sum of individual peroxy radicals [$r^2 = 0.98$], supporting the photochemical theory presented in section 3. The model, however, does a poor job in representing the factors that cause variations about the mean in the measured peroxy radical levels, as seen in the correlation in Figure 3 [$r^2 = 0.27$].

We can explain the relatively weak correlation of Figure 3 with respect to the strong correlation of Figure 2 by noting that the NO/NO_2 ratio is affected by two ma-

jor influences: (1) the ratio determined from the reactions of (R1) and (R2) alone plus (2) a smaller modification from reactions (R3) - (R5) representative of peroxy radical levels. Reactions (R1) and (R2) depend only on NO_x, O_3, and solar intensity. Peroxy radicals, however, involve all of the hydrocarbon chemistry, which is complex and extensive, exceeding the current measurement and modeling capabilities. Consequently, it is no surprise that the model versus measurement correlation of NO/NO_2 is stronger than the correlation of ΣRO_2. In addition, model-calculated ΣRO_2 is driven largely by the rate of the $O_3 + h\nu \longrightarrow O(^1D) + O_2$ photolysis reaction. Estimates for this rate during cloudy periods are approximate. Finally, peroxy radical levels are strongly affected by aqueous reactions not included in the model. Indeed, a day by day examination suggests that the largest differences between measurement and model results occur during periods of fog, rain, and scattered cloud cover, supporting the theory that cloud processes not included in the model (i.e., aqueous chemistry, rain-out, and variations in solar intensity) influence the radical photochemistry at the site.

Surface deposition is not included in the model runs because of uncertainties associated with chemical deposition to the ocean surface within a stable marine boundary layer [e.g., *Voldner et al.*, 1986; *Joffre*, 1988]. However, section 5.8 presents model results that examine the potential effects of including surface deposition in the model calculations. We include neither wet deposition nor aqueous chemistry in the model simulations.

Many authors investigate the impact of chlorine, bromine, and iodine on ozone loss [e.g., *Finlayson Pitts et al.*, 1990; *Singh et al.*, 1996; *Davis et al.*, 1996b]. We have not included halogen chemistry in our model simulations but intend to pursue this topic in future research. The Sable Island data set lends itself well to studying the impact of halogens on ozone photochemistry because the site is located within the marine boundary layer and levels of speciated NMHCs are available at the site throughout the intensive, and their ratios may well provide evidence of halogen atom reactivity.

5. Results and Discussion

5.1. Net Photochemical Ozone Production

Figure 4 presents net photochemical ozone production rates integrated over 24 hours for FIVEMIN model simulations during the 16 days of measurements. Net ozone production [$(P - L)(O_3)$] refers to the difference between ozone production and loss rates [$(P - L)(O_3) = P(O_3) - L(O_3)$]. The average net photochemical ozone production integrated over 24 hours for these simulations is 3.6 ppbv/d ($\sigma = \pm 3.8$ ppbv/d) with a median value of 3.5 ppbv/d. The maximum value, 13.6 ppbv/d, and the minimum value, -2.3 ppbv/d, demonstrate the large variability at the site. These
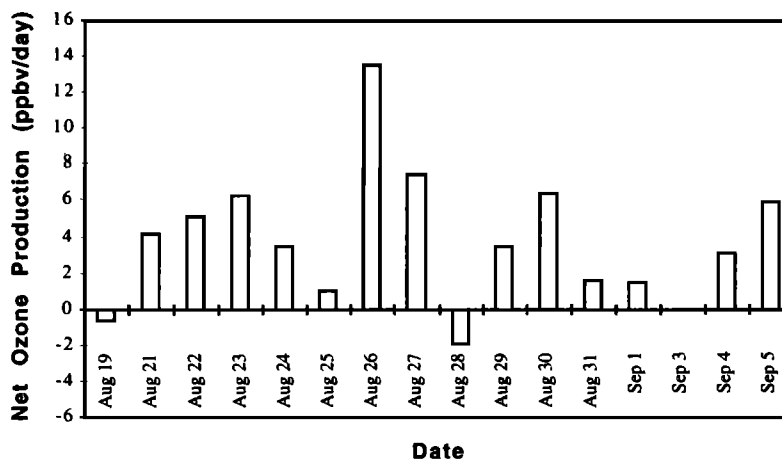
Figure 4. $(P - L)(O_3)$ integrated over 24 hours for the FIVEMIN simulations.

model simulations indicate net photochemical ozone production at the site for all days save three: August 19, August 28, and September 3. All three of these days exhibit low levels of solar radiation (51, 59 and 66% of the clear-sky maximum, respectively) and low levels of NO_x (53, 61 and 53% of the median values, respectively).

There are 3 days exhibiting NO_x levels that are significantly higher than the campaign median of 97 pptv (Tables 1 and 2): August 21, August 26, and September 5. Selected alkane levels (propane, alk4, and alk7) are also high on these days (Table 2). On all three of these days, surface winds are from the southwest in the direction of the oil platform. In particular, there is a NO_x peak on August 21 in the late morning that reaches 7 ppbv with high NO_x/NO_y ratios (0.8-1.0) suggesting a fresh source upwind of the measurement site. If we exclude these 3 days from the data set, the average net photochemical ozone production (FIVEMIN simulations) is 2.7 ppbv/d.

As described in section 4, there are three types of simulations presented in this study involving: (1) high-resolution input (FIVEMIN), (2) 1000-1400 LT median values as input (MEDIAN) and (3) 1000-1400 LT mean values as input (MEAN). Figure 5 compares net photochemical ozone production integrated over 24 hours from these sets of simulations. It is evident that the resolution of input values and the particular method of averaging introduce significant differences. Calculations based on high-resolution data (FIVEMIN) result in significantly higher photochemical ozone production on some days (e.g., August 23, August 28, August 30, and September 4) and significantly lower production on other days (e.g., August 21 and September 5). This difference is due in large part to three factors, all resulting from peaks in NO_x. First, intermittant peaks in measured NO_x create a situation in which the median values are significantly lower than the mean values, resulting in differences in photochemical ozone production (August 26). Second, large peaks in NO_x levels before and after
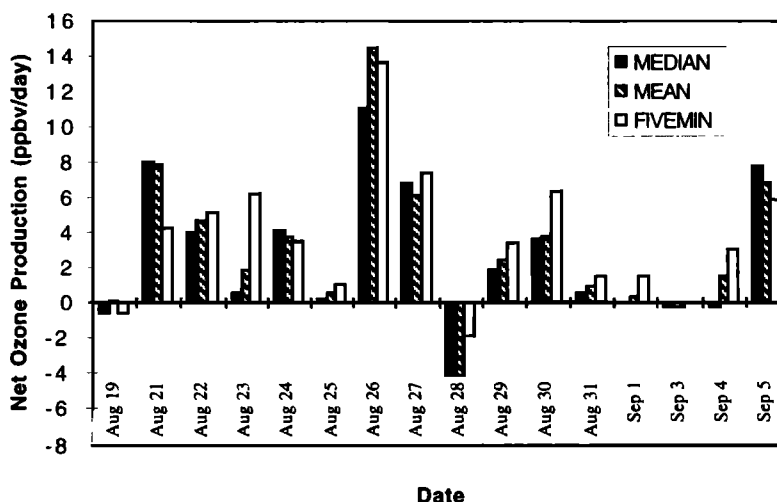

Figure 5. Comparison of $(P - L)(O_3)$ integrated over 24 hours for FIVEMIN, MEDIAN and MEAN simulations.

the 1000-1400 LT time window occasionally introduce differences between the FIVEMIN and the MEDIAN and MEAN results (e.g., August 23, August 28, August 30, and September 4). The third reason concerns large peaks in NO_x within the 1000-1400 LT time window (e.g., August 21 and September 5). Because ozone production efficiency decreases with increasing NO_x levels [e.g., *Liu et al.*, 1987; *Lin et al.*, 1988; *Sillman et al.*, 1990b; *Chatfield and Delany*, 1990], averaging over NO_x peaks by using either the 1000-1400 LT mean or median values would tend to overpredict O_3 production rates.

5.2. Regional Ozone Photochemistry

In this section we use the MEDIAN simulations which filter out peaks in NO_x in an effort to present results more characteristic of regional photochemistry. The average value of net ozone production integrated over 24 hours derived for the 16 days using these simulations is 2.7 ppbv/d ($\sigma = \pm 4.0$). The contributions to photochemical ozone production and loss rates from reactions (R3) - (R5) and (R6) - (R8), respectively, appear in Figure 6 (instantaneous noontime values, ppbv/hour). On average, the conversion of NO to NO_2 by HO_2 is responsible for 46% of the photochemical ozone production.

The conversion of NO to NO_2 by CH_3O_2 is responsible for 19%, and the reaction of NO with other organic peroxy radicals is responsible for 35%. The significant oxidation of NO to NO_2 by organic peroxy radicals other than CH_3O_2 indicates the importance of NMHC levels in photochemical ozone production at the site (section 5.4).

Ozone photochemical loss rates are dominated by the photolysis of ozone followed by the reaction of $O(^1D)$ with water vapor. On average, over 64% of ozone photochemical loss occurs through this net reaction. The reaction of ozone with HO_2 contributes 28% to ozone photochemical loss, and the reaction of ozone with OH contributes 7%.

Assuming that these results are characteristic of regional photochemistry, the correlations of model-calculated photochemical ozone production and loss rates with input parameters provide information about the factors controlling ozone photochemistry in the region. Photochemical ozone production increases strongly with NO_x in model calculations. To a lesser extent, photochemical ozone production increases with solar intensity and NMHCs. Ozone loss rates increase strongly with increasing levels of ozone and solar in-
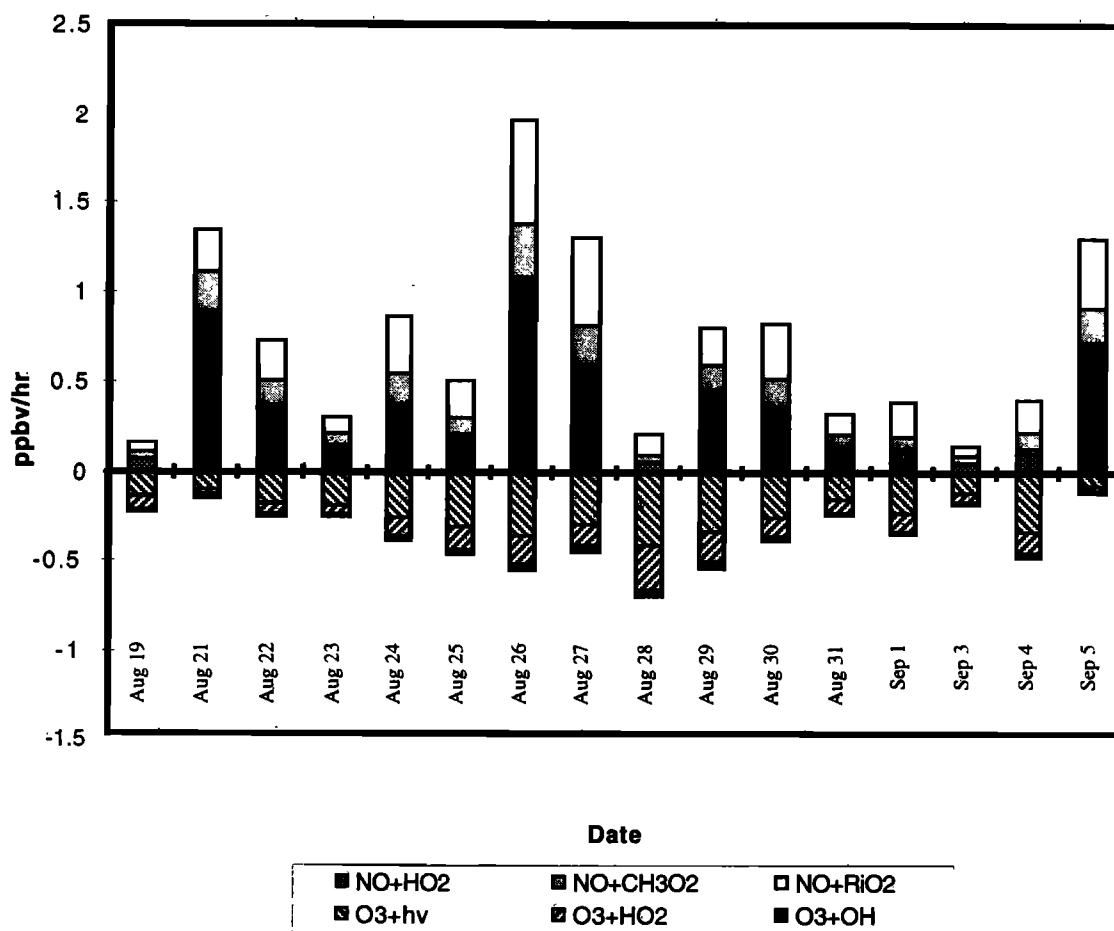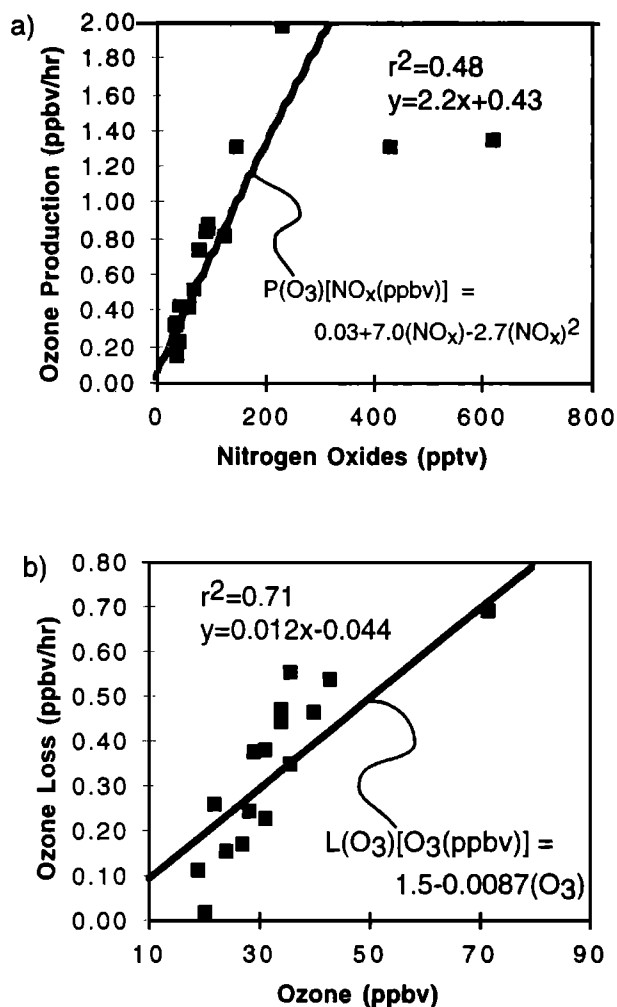

Date

■ NO+HO2	▨ NO+CH3O2	▢ NO+RiO2
▨ O3+hv	▨ O3+HO2	■ O3+OH

Figure 6. Instantaneous rates of $P(O_3)$ and $L(O_3)$ from (R3)-(R5) and (R6)-(R8), respectively, using MEDIAN simulations.

a)

$r^2=0.48$
$y=2.2x+0.43$

$P(O_3)[NO_x(ppbv)] =$
$0.03+7.0(NO_x)-2.7(NO_x)^2$

Ozone Production (ppbv/hr)

Nitrogen Oxides (pptv)

b)

$r^2=0.71$
$y=0.012x-0.044$

$L(O_3)[O_3(ppbv)] =$
$1.5-0.0087(O_3)$

Ozone Loss (ppbv/hr)

Ozone (ppbv)

Figure 7. Calculated instantaneous rates of (a) production of ozone at noon versus measured NO_x and (b) loss of ozone versus measured O_3 based on model calculations for each of the 16 days (squares). The lines show $P(O_3)$ versus NO_x and $L(O_3)$ versus O_3 based on model calculations using the campaign averages for all input parameters (Table 1) except for NO_x and O_3, respectively. Excluding the two outliers of August 21 and September 5 from Figure 7a gives $r^2 = 0.94$, slope equal to 8.9 and y intercept equal to -0.07.

tensity. Figure 7 shows the correlations of noontime photochemical ozone production with NO_x and ozone loss rates with O_3 from the model runs. As shown in this figure, the rate of ozone production is closely correlated with NO_x on all days except for two outliers (August 21 and September 5), both days with dense cloud cover. Net photochemical ozone production also increases with increasing levels of NO_x. Ninety-five percent of the NO_x measurements at the island fall between 19 and 881 parts per trillion by volume (pptv), indicating the potential for net photochemical ozone production as well as net ozone loss.

It is important to acknowledge the dangers of extrapolating in situ results from this data set to conclusions concerning regional photochemistry and climatology. First, the synoptic flow over the island dur-

ing the NARE 1993 summer intensive is anomalous, with frequent flow from the clean continental areas to the northwest rather than from the polluted regions to the southwest [*Merrill and Moody*, 1996; *Moody et al.*, 1996]. Second, the measurement site is located within the marine boundary layer, assumed to be thermally stable during periods of flow from the polluted continent [e.g., *Wang et al.*, 1996; *Angevine et al.*, 1996]. Consequently, air masses sampled at the site are not necessarily of the same origin as indicated by synoptic flow [e.g., *Angevine et al.*, 1996; *Kleinman et al.*, 1996; *Daum et al.*, 1996]. Current research involving this data set focuses on chemical correlations based on air mass origin determined from synoptic flow as well as an analysis of the local meteorology using vertical soundings and surface observations to determine whether or not surface observations are characteristic of flow aloft (M.A. Carroll et al., manuscript in preparation, 1998). Third, as discussed in section 5.4, there is some evidence of hydrocarbon variability, resulting from local emissions (especially isoprene), which may influence photochemical ozone production rates. Finally, high variability in NO_x attributed to polluted plumes from ship traffic and the oil platform to the southwest [*Wang et al.*, 1996] may lead to significantly different values of photochemical ozone production at the site than would be expected on a regional scale.

Local sources are also suggested by high NO_x/NO_y ratios concurrent with peaks in NO_y [*Wang et al.*, 1996]. Ship traffic may represent a characteristic source of the western North Atlantic. On the other hand sources such as the oil platform would be unique to Sable Island. The median ratio of NO_x/NO_y at Sable Island is 0.3. In contrast, aircraft measurements taken in the lowest 1.5 km over the Gulf of Maine show values of NO around 50 pptv and NO_y around 1 ppbv [*Buhr et al.*, 1996]. If we assume a noontime NO/NO_2 ratio similar to the median NO/NO_2 ratio at Sable Island (0.3), we arrive at a NO_x/NO_y ratio over the Gulf of Maine of 0.2. Similarly, aircraft measurements in the polluted continental plume give median NO_x/NO_y ratios of 0.16 [*Daum et al.*, 1996]. The higher NO_x/NO_y ratios at Sable Island could suggest (1) a local source of NO_x unique to the location, (2) different transport regimes to Sable Island than to the regions sampled by the aircraft, (3) more significant loss of NO_y through deposition and cloud chemistry within air masses transported to Sable Island, or (4) release of NO_x due to thermal decomposition of PAN following diabatic heating over Sable Island.

5.3. Net Photochemical Ozone Production and Air Mass Origin

Carroll et al. [1994] discuss the variation of chemical mixing ratios in air masses with different synoptic origins. Figure 8 shows calculated net photochemical ozone production integrated over 24 hours during events grouped into three categories of air mass ori-
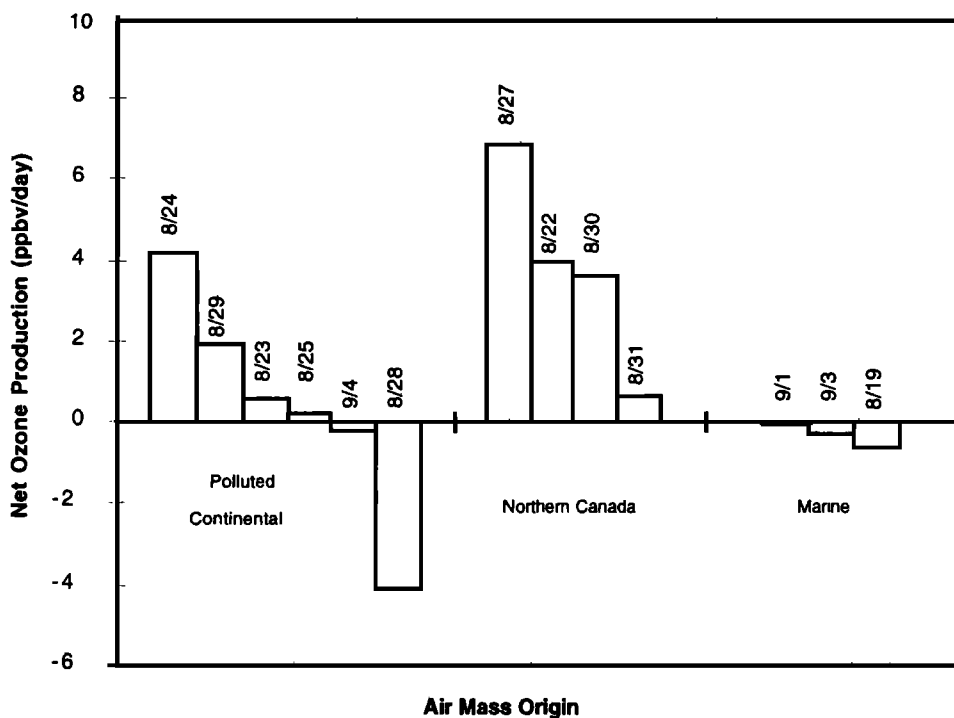
Figure 8. $(P - L)(O_3)$ integrated over 24 hours (MEDIAN simulations) in categories of synoptic air mass origin.

gin: marine, northern Canada, and polluted continental. We consider values of net ozone production resulting from model calculations using the MEDIAN simulations in order to present results more characteristic of regional photochemistry (as in section 5.2). We have excluded August 21, August 26, and September 5 from this analysis because the NO_x, aerosol, surface wind direction, and alkane levels indicate probable contamination of the air masses from local sources such as the oil platform to the southwest (section 5.1). We have excluded these days in order to form more conservative conclusions on the impact of flow from the continent on the chemistry of the region. August 21 $[(P - L)(O_3) = 8.0$ ppbv/d] is characterized by synoptic scale transport from the marine regions to the east but surface winds from the southwest. August 26 $[(P - L)(O_3) = 11$ ppbv/d] represents a day of transition of synoptic flow from the polluted continental to northern Canada regions with surface winds from the southwest. September 5 $[(P - L)(O_3) = 7.8$ ppbv/d] indicates an air mass origin from the polluted continent with surface winds from the southwest.

The groupings show evidence that in situ ozone production is highest in air masses which originate from northern Canada rather than from the more polluted regions of eastern North America. This is most likely due to the impact of NO_x emission sources in Nova Scotia, relatively close to Sable Island. As described in section 5.2, ozone production rates are primarily dependent on NO_x levels, while ozone loss is determined largely by

ozone levels. Significant net production of ozone is calculated only during events with NO_x greater than 70 pptv. These events are more frequently associated with transport from northern Canada than transport from the polluted continental region. Air masses originating from the polluted continental region tend to have relatively low NO_x (Table 2), presumably because of NO_x removal during transport. The polluted air masses also tend to have higher ozone, especially on August 28. The combination of high ozone and low NO_x creates a situation in which polluted continental air masses at Sable Island may be characterized by net ozone loss rather than production. Furthermore, transport from the polluted continental region is frequently accompanied by cloud cover, which limits ozone production even when NO_x is present (August 29).

As mentioned in section 5.2, the flow regimes characterizing the NARE summer intensive are anomalous [*Merrill and Moody*, 1996]. Climatologically, circulation around the Bermuda High brings air from the urban corridor along the east coast of the United States to Sable Island in summer [*Wendland and Bryson*, 1981]. During this period of measurements at Sable Island, however, only 30% of the flow originates over the polluted continent, with only one pollution episode attributable to flow from the eastern United States [*Wang et al.*, 1996]. As a consequence, the results of this photochemical modeling study may not adequately represent climatological trends of photochemical ozone production at the site during the month of August.

Table 3. Noontime OH Mixing Ratios and OH Reactions With CO, CH_4, and NMHCs Using 1000-1400 LT Median Values

	Mean ($\pm\sigma$)	Median	Maximum	Minimum
OH, mol cm^{-3}	3.3×10^6 ($\pm 1.0 \times 10^6$)	3.5×10^6	5.4×10^6	1.6×10^6
CO + OH, ppbv/h	0.35 ($\pm$0.16)	0.35	0.75	0.15
CH_4 + OH, ppbv/h	0.11 ($\pm$0.03)	0.11	0.18	0.05
Alkanes + OH, ppbv/h	0.02 ($\pm$0.02)	0.01	0.08	0.006
Alkenes + OH (all but isoprene), ppbv/h	0.03 ($\pm$0.02)	0.02	0.10	0.01
Isoprene + OH, ppbv/h	0.07 ($\pm$0.04)	0.07	0.18	0.01
Aromatics + OH, ppbv/h	0.01 ($\pm$0.01)	0.01	0.02	0.002

5.4. Nonmethane Hydrocarbons and Anthropogenic Impact

Possible sources of nonmethane hydrocarbons include long-range transport from the continent, emissions from passing ships or the oil platform to the southwest, oceanic emissions, and local emissions from the island. Unfortunately, the resolution of nonmethane hydrocarbon measurements is insufficient to resolve the observed variability. We have filtered the NMHC measurements according to evidence of local pollution subjectively inferred from anomalous peaks (several orders of magnitude above average values) in aerosols, NO_x (according to Wang et al. [1996]), and NMHCs. Some evidence of contamination in several collection canisters by ethene, propene, benzene, and toluene further reduces the number of observations available for this study.

Table 3 shows the significance of NMHCs to photochemical ozone production by comparing the instantaneous noontime production rates of OH reactions with CO, CH_4, and NMHCs (using MEDIAN simulations). Hydroxyl radical reactions generally initiate the oxidation sequence of these compounds with subsequent reactions resulting in the formation of peroxy radicals and consequently photochemical ozone production. On average, the reaction of CO with OH at noon proceeds at a rate of 0.35 ppbv/h, the reaction of CH_4 with OH proceeds at 0.11 ppbv/hr and the total of the reactions of NMHCs with OH proceeds at 0.16 ppbv/h. It is clear that NMHCs contribute significantly to photochemical ozone production relative to CO and CH_4. In contrast, at other oceanic sites more removed from continental influence, NMHCs are assumed to play a negligible role in photochemical ozone production [e.g., Liu et al., 1983; Chameides et al., 1987; Ridley et al., 1992]. However, it is important to differentiate between site specific photochemistry and regional photochemistry. At Sable Island, levels of alkenes (including isoprene) and aromatics, both having short lifetimes, may represent local sources.

We present the contribution of speciated hydrocarbons to photochemical ozone production at the site using an OH-reactivity-based scale developed by Chameides et al. [1992]. In this scale the reactivity of a given hydrocarbon with OH is normalized to the reactivity of propene in pptv:

$$\text{propene} - \text{equivalent(j)} = [X_j]\frac{C_j}{3}\frac{k_{OH}(j)}{k_{OH}(C_3H_6)} \quad (5)$$

where $[X_j]$ is the mixing ratio of a particular hydrocarbon species j in pptv, C_j is the number of carbon atoms in j, 3 is the number of carbon atoms in propene, and $k_{OH}(j)$ and $k_{OH}(C_3H_6)$ are reaction rates of j and propene with respect to OH, respectively. Unlike the forward production rates from OH reactions, this approximation takes into account the number of carbon atoms oxidized from each hydrocarbon molecule. Table 4 presents a ranked list of propene-equivalent mixing ratios of nonmethane hydrocarbons for mean values of the Sable Island data set.

The reactivity of isoprene in Table 4 calls into question local island influences. The lifetime of isoprene with respect to OH calculated at noon averages 1 hour (range 0.6-2.1 hours). According to back trajectory calculations, transport times from the continent to the island range from several hours, when the air mass passes directly over Nova Scotia, to several days, for other air mass origins [Merrill and Moody, 1996]. It is unlikely that isoprene emitted from the continent would survive transport over the ocean to the island. Furthermore, the pronounced diurnal variation in isoprene levels suggests local sources. During daytime (0800-1600 LT) isoprene mixing ratios average 71 pptv (median equal to 55 pptv, $\sigma = \pm 51$ pptv, n = 35). At night (2000-0400 LT) isoprene mixing ratios average 16 pptv (median equal to 9 pptv, $\sigma = \pm 23$ pptv, n = 16). The island lacks trees, the strongest emitters of isoprene, but is covered by grasses and succulent plants, weak emitters of isoprene [Lamb et al., 1987]. Estimated isoprene emissions of 0.2 mg C m^{-2} h^{-1}, a conservative estimate with respect to the rates used by Guenther et al. [1995] to model emissions in low productivity grass and shrublands, would result in ambient mixing ratios of the order of 100 pptv [Guenther et al., 1996], comparable to observations at Sable Island. Although the ocean may also represent a potential source of isoprene [Bonsang et al., 1992], an oceanic source is unlikely because of the variabil-

Table 4. Propene-Equivalent Mixing Ratios of Nonmethane Hydrocarbons for August 22 (Clear Sky) and August 28 (Fog)

Hydrocarbon, pptv	August 22		August 28	
	Mixing Ratio	Propene-Equivalent	Mixing Ratio	Propene-Equivalent
Isoprene	235	940	565	2278
Toluene	826	202	805	200
Propene	177	177	162	162
Alk4[a]	729	68	1490	143
Ethene	140	46	138	45
Benzene	444	20	1092	51
Propane	468	18	1164	45
Ethane	1728	14	2800	24
Alk7[b]	60	13	36	8

[a]Denotes n-butane, i-butane, n-pentane, and i-pentane.
[b]Hexane.

ity of isoprene levels, a feature expected for emissions from island vegetation but not for a widespread oceanic source.

Selected alkenes (e.g., propene) and aromatics (e.g., toluene) are also highly reactive in the model simulations. We assume that these short-lived anthropogenic hydrocarbons originate from local anthropogenic sources: the island generator, passing ships, the oil platform to the southwest, or sources from Nova Scotia. Several hydrocarbon samples on August 24, August 26, and September 5 show evidence of emissions from liquified petroleum gas, suggesting anthropogenic influences from the island. Categorizing the data according to air mass origin does not show significant trends in levels of these hydrocarbons. This result is most likely due either to local sources of NMHCs or to uncertainties associated with assigning categories of air mass origin to the chemical data set.

In light of concerns that alkenes (including isoprene) and aromatics observed at the site may come from local sources, we present model simulations (FIVEMIN) in which (1) we include all NMHCs, (2) we exclude isoprene but retain other NMHCs, (3) we exclude all alkenes and aromatics but retain alkanes, and (4) we exclude all NMHCs. Simulations 3 and 4 do not assume initial concentrations of alkenes, aromatics, and the derivatives acetone and methyl ethyl ketone during the model spin-up period. The simulations which take into account all NMHC species measured at the site give an average net photochemical ozone production rate integrated over 24 hours of 3.6 ppbv/d ($\sigma = \pm 3.8$). Results from simulations excluding isoprene average 2.9 ($\sigma = \pm 3.3$). Results from simulations excluding alkenes and aromatics average 2.0 ($\sigma = \pm 2.7$). Finally, results from simulations excluding all hydrocarbons average 1.6 ($\sigma = \pm 2.3$). A similar set of results based on MEDIAN simulations that tend to filter out NO_x peaks leads to the following results (1) all NMHCs (average equal to 2.7 ppbv/d, $\sigma = \pm 4.0$), (2) no isoprene (average equal

to 2.0 ppbv/d, $\sigma = \pm 3.5$), (3) no alkenes and aromatics (average equal to 1.6 ppbv/d, $\sigma = \pm 3.0$), (4) no NMHCs (average equal to 1.1 ppbv/d, $\sigma = \pm 2.5$). Consequently, there is a range of 1-4 ppbv/d that could represent regional values of net ozone production.

If levels of isoprene are indeed an island effect and other alkenes and aromatics result from local sources, the simulation excluding alkenes and aromatics using median 1000-1400 LT input would provide the most reasonable estimate for O_3 production and loss rates for the region, giving an average net ozone production rate integrated over 24 hours of 1.6 ppbv/d. It is clear from Tables 3 and 4 that without alkenes and aromatics the chemistry would be dominated by CO and CH_4. Indeed, noontime instantaneous production rates of OH reactions for the simulations that exclude alkenes and aromatics average the following: CO + OH (0.49 ppbv/h), CH_4 + OH (0.15 ppbv/h) and alkanes + OH (0.03 ppbv/h). Furthermore, in these simulations the noontime instantaneous production rate of the reaction of OH with other organic gases derived from alkane oxidation (acetaldehyde, higher aldehydes, acetone, methyl ethyl ketone, and methanol) averages only 0.03 ppbv/d. The reaction of formaldehyde, which results from both CH_4 and alkane oxidation, proceeds at an average rate of 0.07 ppbv/h. While the oxidation of alkanes and their derivatives is significant in these simulations, it does not equal the influence of CO and CH_4 oxidation on O_3 production.

5.5. NO/NO_2 Ratios

Peak NO/NO_2 ratios calculated from MEDIAN model simulations and using all NMHCs measured at the site average 0.33 for the 16 days used in this study (median equal to 0.31, maximum equal to 0.57, minimum equal to 0.12, $\sigma = \pm 0.10$). These values are lower than ratios observed in the marine boundary layer over the North Pacific during Chemical Instrumentation Test and Evaluation (CITE) 2, ranging from 0.7

to 1.0 [*Carroll et al.*, 1990], as well as model and measurement analyses for free tropospheric flow at Mauna Loa, averaging approximately 0.6 at noon [*Ridley et al.*, 1992]. The lower NO/NO$_2$ ratios at Sable Island result from the combination of higher O$_3$ levels as well as lower levels of solar intensity, noting that cloudy days are included in the Sable Island analysis. NO/NO$_2$ ratios from model calculations for the most part agree with observations (Figure 2). However, differences on smaller timescales occur during periods of fog and/or precipitation, as discussed in section 5.7.

5.6. Peroxy Radicals

Noontime peak total peroxy radical mixing ratios average 39 pptv for the MEDIAN model simulations using all NMHCs measured at the site (median equal to 41 pptv, maximum equal to 63 pptv, minimum equal to 12 pptv, $\sigma = \pm 16$). These levels are slightly lower than noontime average levels of peroxy radicals calculated during other summertime modeling studies in remote and rural locations such as the lower free troposphere over Mauna Loa, 50 pptv [*Ridley et al.*, 1992], the boundary layer air sampled at Niwot Ridge, 60 pptv equivalent [*Parrish et al.*, 1986], and Scotia, Pennsylvania, 70-218 pptv [*Trainer et al.*, 1991]. They are also lower than calculations of noontime peroxy radicals from measurements made at Mauna Loa, 60 pptv [*Ridley et al.*, 1992], as well as the direct measurements of peroxy radicals made at Izaña (Canary Islands), 50-100 pptv [*Mihelcic et al.*, 1994].

The noontime ratio of hydroperoxy radicals to total peroxy radicals (HO$_2$/$\sum$RO$_2$) calculated for the Sable Island dataset averages 0.46 over the sixteen days (median = 0.45, max = 0.66, min = 0.28, $\sigma = \pm$ 0.10). These model results are similar to measurements at Izaña, which give ratios around 0.5 [*Mihelcic et al.*, 1994]. The Sable Island ratios are slightly higher than ratios determined from photochemical models at Scotia, averaging 0.3 [*Trainer et al.*, 1991], and slightly lower than ratios determined from models at Mauna Loa [HO$_2$/(HO$_2$+CH$_3$O$_2$)], averaging 0.6 [*Ridley et al.*, 1992].

The model partitioning of organic peroxy radicals provides an additional means of assessing the contribution of speciated NMHCs to photochemical ozone production rates. Table 5 lists results from 2 days of model simulation: August 22, a clear-sky day representative of relatively clean air, and August 28, a cloudy day during the peak of the pollution episode. For August 22, RIO$_2$ (isoprene peroxy radical) and VRO$_2$ (methyl vinyl ketone peroxy radical), both intermediates of isoprene oxidation, comprise 34% of R$_i$O$_2$ (the total organic peroxy radicals excluding CH$_3$O$_2$). An analysis of the production rates of RIO$_2$ with NO and VRO$_2$ with NO suggests that these two derivatives of isoprene are responsible for approximately 9% of the photochemical ozone production modeled at the site. Of course, the

Table 5. Model Partitioning of Organic Peroxy Radicals for August 22 and August 28
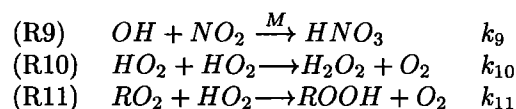
Peroxy Radical, pptv	August 22	August 28
HO$_2$	18.2	17.9
MO$_2$	7.0	11.8
R$_i$O$_2$ (sum)	9.6	32.6
PO$_2$	3.5	9.2
RIO$_2$	2.5	10.8
MCO$_3$	1.9	3.0
VRO$_2$	0.8	1.0
GCO$_3$	0.6	3.5
ETO$_2$	0.4	1.2
ECO$_3$	0.4	2.0

Model nomenclature from *Lurmann et al.* [1986]: HO$_2$, hydrogen peroxy radical; MO$_2$, methyl peroxy radical; R$_i$O$_2$, sum of organic peroxy radicals other than MO$_2$; PO$_2$, propene peroxy radical; RIO$_2$, isoprene peroxy radical; MCO$_3$, peroxyacetyl radical; VRO$_2$, methyl vinyl ketone peroxy radical; GCO$_3$, HOCH$_2$CO$_3$; ETO$_2$, C$_2$H$_5$O$_2$; ECO$_3$, organic CO$_3$ compounds derived from higher NMHCs.

oxidation mechanism of isoprene also increases levels of HO$_2$ and CH$_3$O$_2$, leading to an additional indirect contribution to photochemical ozone production. Similarly, for August 28, RIO$_2$ and VRO$_2$ comprise 36% of R$_i$O$_2$, suggesting a contribution to photochemical ozone production of approximately 17%. Results from both days indicate the importance of isoprene in photochemical ozone production at the site.
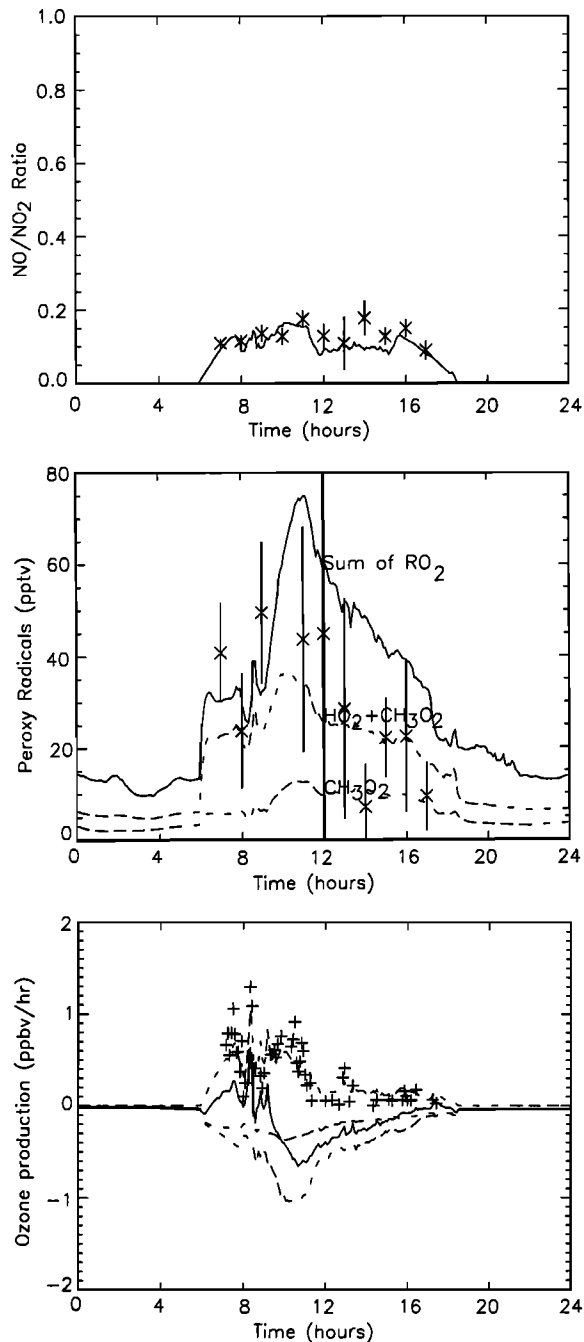
5.7. Case Studies During Fog and Rain

During episodes of fog and rain, aqueous chemistry and rainout may influence chemical concentrations and forward production rates not captured by the gas-phase mechanism of the model. Consider the following termination reactions for peroxy radicals:

(R9)	$OH + NO_2 \xrightarrow{M} HNO_3$	k_9
(R10)	$HO_2 + HO_2 \longrightarrow H_2O_2 + O_2$	k_{10}
(R11)	$RO_2 + HO_2 \longrightarrow ROOH + O_2$	k_{11}

The products of reactions (R9) and (R10) are highly soluble in water, with Henry's law coefficients at 25°C of 2.1 x 10^5 [*Schwartz and White*, 1981] and 6.9 x 10^4 [*Hwang and Dasgupta*, 1985], respectively. Removal of HNO$_3$ and H$_2$O$_2$ from the system through rainout decreases levels of peroxy radicals and nitrogen oxides. Because the latter species are catalysts for ozone production, reducing their concentrations decreases the efficiency of ozone production.

Other loss processes could involve the dissolution of peroxy radicals, HNO$_3$, and H$_2$O$_2$ into fog droplets followed by aqueous reactions and subsequent reevaporation [e.g., *Lelieveld and Crutzen*, 1990; *Carroll et al.*, 1994; *Norton et al.*, 1994; *Roberts et al.*, 1996]. *Roberts et al.* [1996] present measurements of NO$_y$ at Chebogue
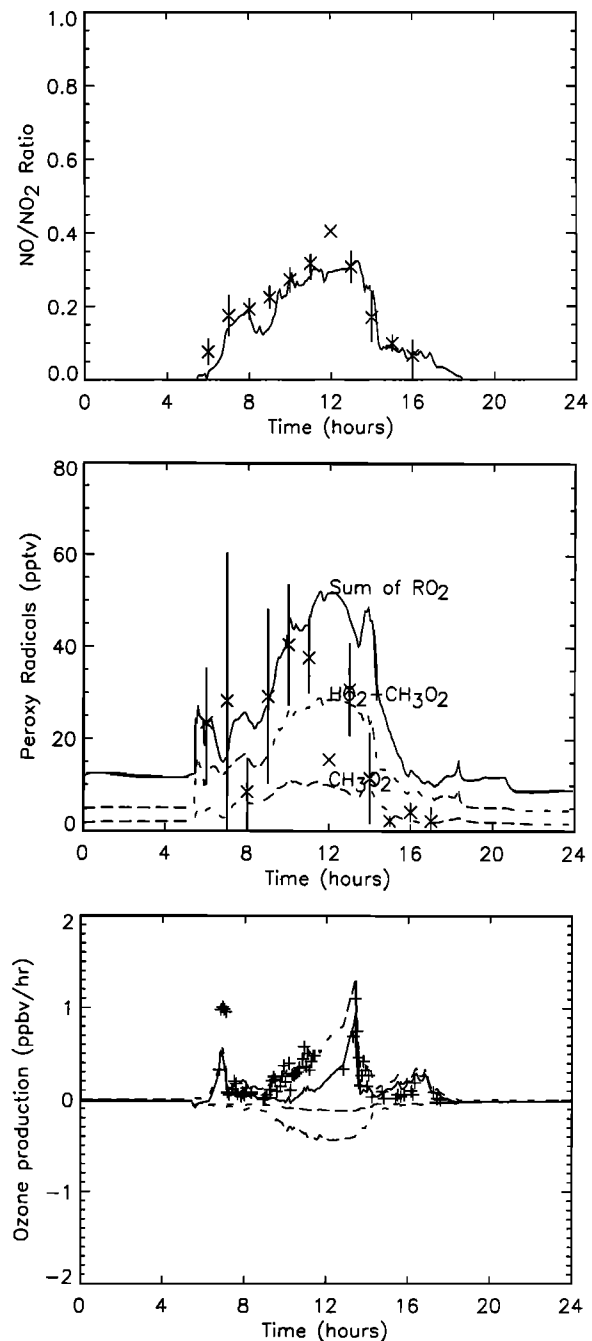
NO$_x$ has been proposed to occur in liquid and solid aerosol processes [*Hauglustaine et al.*, 1996; *Jacob et al.*, 1996].

Surface observations on 6 out of the 16 modeled days record rain or drizzle during daylight hours. These are prime conditions for the loss of HNO$_3$ and H$_2$O$_2$ through rainout. Fog was present on 8 of the 16 days used in this analysis. Four of these days record observations of both fog and rain. There is also the possibility of the chemical loss of intermediate species through rainout and fog during transport from the continent to the island.

Figure 9. Model results for August 28. (a) NO/NO$_2$ ratios. (b) Peroxy radical mixing ratios: Total peroxy radicals (solid line); HO$_2$ + CH$_3$O$_2$ (dotted line); CH$_3$O$_2$ (dashed line). (c) Ozone production: (P − L)(O$_3$) (solid line); P(O$_3$) (dotted line); L(O$_3$) (broken line); ozone loss by reaction with HO$_2$ (dashed line). Hourly mean values (crosses) and standard deviations (vertical bars) of measurements also appear on the figure. Fog is present throughout the day.

Point and Sable Island as well as speciated NO$_y$ at Chebogue Point to show evidence of wet deposition and cloud chemistry in air masses reaching these sites. They suggest that the loss of peroxy acetyl nitrate (PAN) correlates with fog episodes, providing an additional mechanism for NO$_y$ loss. Furthermore, cycling of HNO$_3$ to

Figure 10. As in Figure 9 but for September 1. Rain and fog are present throughout the afternoon and evening.

Figures 9 and 10 present model results (FIVEMIN) for August 28 and September 1. Figure 11 shows the results of a clear-sky day, August 22, for comparison. Surface observations indicate the presence of fog throughout the day on August 28 and in the afternoon and evening of September 1. No rain is reported on August 28, but rain accompanies the fog on September 1. For both days, peroxy radicals calculated using measurements are 30% lower than those calculated by the numerical model during periods of rain or fog. During periods of rain or fog the model tends to calculate larger values of peroxy radicals than values derived from mea-

Figure 11. As in Figure 9 but for August 22. Clear skies prevail throughout the day.

surements. September 3 (not shown) is an exception, but model results still fall within the large variability of peroxy radicals calculated from measurements, presumably caused by the rapid fluctuations in solar intensity measured on that day. August 22, an example of a day with clear sky observations, shows considerably closer agreement among model calculations and values calculated from measurements.

Given the prevalence of fog and rain at the site, it would be worthwhile to include aqueous reactions and rain out in the model. Results of box model studies by *Lelieveld* [1990] give a rough estimate of the influence that aqueous reactions might have on photochemistry in this location. *Lelieveld* [1990] uses longitudinally averaged conditions at 45°N north latitude and 1.5 km altitude to calculate a summertime net ozone production of +3.3 ppbv/d with gas-phase chemistry alone and +2.3 ppbv/d including aqueous reactions, suggesting a 30% bias when aqueous chemistry is excluded.

5.8. Surface Deposition

The meteorology associated with this data set suggests a stable marine boundary layer created by the flow of warm air over the cool ocean [*Angevine et al.*, 1996], justifying the assumption that the main resistance to surface deposition results from large-scale dynamics associated with atmospheric stability. Considering the complexity of determining deposition velocities over the ocean as well as the strong stability of the atmosphere in this region, we assume deposition to be negligible for the in situ photochemical calculations presented up to this point.

Surface deposition appears in the box model as an additional sink:

$$\frac{d[C_i]}{dt} = \frac{v_d[C_i]}{h} \tag{6}$$

where C_i is the concentration of the species, v_d is the deposition velocity, and h is the model height. Our analyses of vertical soundings over Sable Island during the intensive suggest internal boundary layer or marine boundary layer thicknesses ranging from 200 to 1000 m. In this section we assume a model height of 500 m. We consider the maximum impact of including surface deposition on the steady state photochemical calculations by considering depositon velocities (Table 6) taken from the literature [*Liu et al.* 1983; *Thompson and Zafiriou*, 1983; *Sillman et al.*, 1993].

Including surface deposition characteristic over the ocean [*Thompson and Zafiriou*, 1983; *Liu et al.*, 1983] results in an average decrease in net ozone production rates of 7%. The impact of surface deposition is almost entirely due to the loss of H_2O_2, which is allowed to accumulate in the model steady state calculation during the 5 days of model integration time before the results are recorded. When deposition is not included, H_2O_2 model mixing ratios reach 3 ppbv, and the photolysis of H_2O_2 represents a significant source of radicals. When
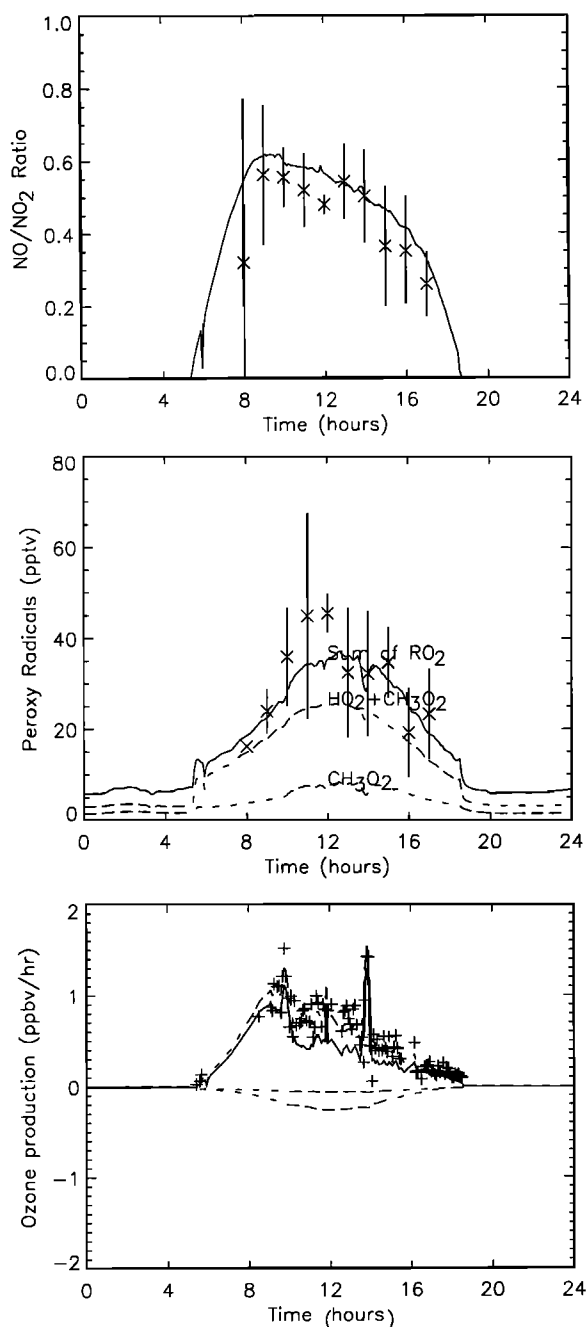
Table 6. Deposition Velocities From the Literature

	Liu et al. [1983]	Thompson and Zafiriou [1983]	Sillman et al. [1993]	
			Over Land	Over Water
O_3	0.05	0.05	0.05	0.6
HNO_3	0.65	0.43	0.05	2.5
NO_2	0.0005	0.0012	0.05	0.6
NO	0.0005	0.00017	0.05	0.1
PAN	0.05	$\cdots$	0.05	0.25
H_2O_2	$\cdots$	0.6	0.05	1

Velocities are in cm s^{-1}

deposition is included, the H_2O_2 values in the model drop below 1 ppbv, and H_2O_2 photolysis is no longer a significant radical source. *Daum et al.* [1996] have measured H_2O_2 mixing ratios of up to 6 ppbv in plumes of polluted air over the North Atlantic off the east coast of the United States, but 1 ppbv is considered a more realistic estimate for H_2O_2 for this region [e.g., *Daum et al.*, 1990; *Lee et al.*, 1993]. OH and HO_2 levels both decrease by 10% in the simulation with surface deposition.

6. Sensitivity and Uncertainty Analysis

Detailed sensitivity studies of chemical mechanisms are available for conditions representative of both urban and rural environments [e.g., *Milford et al.*, 1992; *Yang et al.*, 1995; *Gao et al.*, 1996]. These studies focus primarily on the sensitivity of peak ozone levels to changes in levels of precursor species, meteorological parameters, and reaction rates.

For this study, we conduct a simplified analysis of uncertainties in photochemical ozone production and loss rates for the measurements at Sable Island by considering the uncertainty (precision and accuracy) of the measurements as well as uncertainties intrinsic to the model mechanism. A rough approximation to the sensitivity of photochemical ozone production and loss rates from measurement uncertainties is obtained by holding selected chemical and meteorological input values at their mean value and systematically varying each parameter, x, in order to calculate sensitivity coefficients:

$$\frac{\partial P(O_3)}{\partial x} \qquad (7)$$

The results are presented in Table 7. We use these sensitivity coefficients to determine uncertainties in photochemical ozone production and loss rates inherent to the measurement techniques by means of propogation of errors, a technique that assumes the individual parameters are independent:

$$\sigma^2_{P(O_3)} = \sigma^2_{NOx}\left(\frac{\partial P(O_3)}{\partial NO_x}\right)^2 + \sigma^2_{J_{NO_2}}\left(\frac{\partial O_3 P}{\partial J_{NO_2}}\right)^2 + \ldots \qquad (8)$$

The assumption that the variables used in this analysis are independent is valid for all chemical species except for O_3 and CO, which show a significant correlation [*Wang et al.*, 1996]. J_{NO_2} and temperature show similar diurnal variability, peaking in the middle of the day. However, the dominant factors in photochemical ozone production and loss rates (NO_x, J_{NO_2}, and O_3) are for the most part independent of one another in the complete data set [*Wang et al.*, 1996].

The uncertainties derived from this analysis are presented in Table 8. On the basis of measurement uncertainties of NO_x, J_{NO_2}, NMHCs, O_3, CO, and temperature, photochemical ozone production rates have a 1 σ uncertainty of ±33% (±39% for overcast conditions), photochemical ozone loss rates have a 1 σ uncertainty of ±11% (±23% for overcast conditions), and net photochemical ozone production rates have a 1 σ uncertainty of ±44% (±49% for overcast conditions). It is important to recognize that uncertainties for net ozone production are large in percentage because net ozone production represents a small difference between ozone production and ozone loss rates. However, uncertainties less than 100% validate our conclusions that daytime net ozone production is dominant at the site during the campaign.

In this sensitivity analysis, photochemical ozone production at Sable Island during the intensive depends most strongly on uncertainties in the measurements of NO_x, NMHCs, and solar radiation. Photochemical ozone loss at the site depends primarily on uncertainties associated with measurements of ozone, solar intensity, and relative humidity. Net photochemical ozone production depends on uncertainties associated with measurements of NO_x and to a lesser degree NMHCs, solar radiation, and ozone.

It is beyond the scope of this paper to include an uncertainty analysis of the rate constants in the photochemical model. *Yang et al.* [1995] present a thorough analysis of this type for urban conditions, arriving at a 1 σ uncertainty in ozone levels of ±20-30%. As the study by *Yang et al.* [1995] uses parameters charac-

teristic of a region of significant photochemical ozone production, we assume that uncertainties in ozone production rates at Sable Island are nearly equivalent to the uncertainties in ozone levels calculated by *Yang et al.* [1995]. Adopting a 1 σ uncertainty in ozone production of $\pm 30\%$ based on reaction rates and a 1 σ uncertainty in ozone production of $\pm 33\%$ ($\pm 39\%$ for overcast conditions) results in a total inherent uncertainty of $\pm 45\%$ ($\pm 49\%$ for overcast conditions).

7. Conclusions

On the basis of the photochemical modeling study presented in this paper, ozone photochemistry at Sable Island during the NARE 1993 summer intensive is characterized by net photochemical ozone production. The dependence of photochemical ozone production on elevated levels of NO_x and NMHCs provides evidence for continental influence on the chemistry of the marine boundary layer over the North Atlantic extending out to Sable Island.

The variability in NO_x, alkenes (including isoprene), and aromatics, however, may indicate local sources such as ship plumes or the oil production platform to the southwest, increasing uncertainty in the magnitude of the regional ozone production. Values of net ozone production integrated over 24 hours in the range of 1 to 4 ppbv/d are consistent with the model and experimental results.

Uncertainties and biases in net photochemical ozone production rates calculated at the site include measurement uncertainties ($\pm 44\%$ clear sky, $\pm 49\%$ cloudy sky), surface deposition (-7%), the potential impact of aqueous chemistry (-30%), and uncertainties inherent in the model mechanism (± 20-30%). Furthermore, using median values of chemical mixing ratios during hours of peak sunlight to drive the model as opposed to higher-resolution 5 min averages results in differences in net photochemical ozone production. On the basis of the sensitivity of net ozone production to the factors mentioned above, we conclude that calculating more accurate net photochemical ozone production rates relies primarily on reducing uncertainties in NO_x measurements and calculated photolysis rates as well as improving the resolution of NMHC measurements.

Model results also present evidence that clouds within the marine boundary layer temper ozone production rates (from solar intensity, cloud chemistry, and rainout), encouraging further study involving the role played by clouds and fog in regulating the oxidizing capacity of the marine boundary layer in this region. The meteorological conditions at Sable Island as well as the discrepancies between numerical model calculations and measurements motivate future studies including aqueous reactions and rainout in modeling the chemistry within air masses reaching the site.

Table 7. Sensitivity of O_3P, O_3L, and $(P-L)(O_3)$ to Uncertainties in NO_x, J_{NO_2}, NMHCs, O_3, Temperature, and CO

Species (x)	Mean Value	σ_x^2	$\frac{\partial P(O_3)}{\partial x}$	$(\sigma_{P(O_3)})^2$	$\frac{\partial L(O_3)}{\partial x}$	$(\sigma_{L(O_3)})^2$	$\frac{\partial (P-L)(O_3)}{\partial x}$	$(\sigma_{(P-L)(O_3)})^2$
NO_x	0.19 ppbv	4.5×10^{-3} ppbv²	6.0 hour⁻¹	0.16	0.11 hour⁻¹	1.0×10^{-4}	5.9 hour⁻¹	0.16
J_{NO_2}	6.8×10^{-3} s⁻¹	...	210 $\frac{(ppbv)(s)}{h}$	...	47 $\frac{(ppbv)(s)}{hr}$	...	160 $\frac{(ppbv)(s)}{h}$	...
...Clear		1.0×10^{-7} s⁻²		4.4×10^{-3}		2.0×10^{-4}		2.6×10^{-3}
...Overcast		1.8×10^{-6} s⁻²		0.079		4.0×10^{-3}		0.046
NMHCs	6.8 ppbC	0.23 ppbC²	0.058 $\frac{ppbv}{(ppbC)(h)}$	8.0×10^{-4}	$-7.0 \times 10^{-4} \frac{ppbv}{(ppbC)(h)}$	1.1×10^{-7}	0.058 $\frac{ppbv}{(ppbC)(h)}$	8.0×10^{-4}
O_3	30 ppbv	6.25 ppbv²	-0.012 hour⁻¹	9.0×10^{-4}	0.011 hour⁻¹	8.0×10^{-4}	-0.019 hour⁻¹	2.3×10^{-3}
Temperature	291 K	1 K²	$3.2 \times 10^{-3} \frac{ppbv}{(K)(h)}$	1.0×10^{-5}	$1.9 \times 10^{-3} \frac{ppbv}{(K)(h)}$	3.6×10^{-6}	$1.4 \times 10^{-3} \frac{ppbv}{(K)(h)}$	2.1×10^{-6}
CO	115 ppbv	625 ppbv²	-9.3×10^{-4} hour⁻¹	5.0×10^{-4}	2.1×10^{-5} hour⁻¹	2.8×10^{-7}	-9.4×10^{-4} hour⁻¹	6.0×10^{-4}
Total								
...Clear				0.17		1.1×10^{-3}		0.17
...Overcast				0.24		4.9×10^{-3}		0.21

Here, σ_x^2 refers to the uncertainties inherent to the measurements (Table 1) (units specified in table); $(\sigma_{P(O_3)})^2$, $(\sigma_{L(O_3)})^2$, and $(\sigma_{(P-L)(O_3)})^2$ refer to uncertainties calculated using equation (7) (units specified in table); $\frac{\partial P(O_3)}{\partial x}$, $\frac{\partial L(O_3)}{\partial x}$, and $\frac{\partial (P-L)(O_3)}{\partial x}$ refer to sensitivity coefficients determined using equation (8) (units of $(\frac{ppbv}{h})^2$).

Table 8. Total Uncertainties in $P(O_3)$, $L(O_3)$, and $(P - L)(O_3)$ Based on Results from Table 6 and Mean Values of $P(O_3)$, $L(O_3)$, and $(P - L)(O_3)$

	$\sigma_{(P-L)(O_3)}$, ppbv/h	Model Results Using Mean Values, ppbv/h	Percent Uncertainty
$P(O_3)$	0.41 (clear) 0.49 (overcast)	1.24	33% (clear) 39% (overcast)
$L(O_3)$	0.033 (clear) 0.070 (overcast)	0.31	11% (clear) 23% (overcast)
$NetO_3P$	0.41 (clear) 0.46 (overcast)	0.94	44% (clear) 49% (overcast)

References

Angevine, W. M., M. Trainer, S. McKeen, and C. Berkowitz, Mesoscale meteorology of the New England coast, Gulf of Maine, and Nova Scotia, *J. Geophys. Res.*, *101*, 28,893-28,901, 1996.

Atherton, C. S., S. Sillman, and J. Walton, Three-dimensional global modeling studies of transport and photochemistry over the North Atlantic Ocean, *J. Geophys. Res.*, *101*, 29,289-29,304, 1996.

Bonsang, B., C. Polle, and G. Lambert, Evidence for marine production of isoprene, *Geophys. Res. Lett.*, *19*, 1129-1132, 1992.

Buhr, M., D. Sueper, M. Trainer, P. Goldan, B. Kuster, and F. Fehsenfeld, Trace gas and aerosol measurements using aircraft data from the North Atlantic Regional Experiment (NARE 1993), *101*, 29,013-29,027, 1996.

Cantrell, C. A., R. E. Shetter, J. G. Calvert, D. D. Parrish, F. C. Fehsenfeld, P. D. Goldan, W. Kuster, E. J. Williams, H. H. Westberg, G. Allwine, and R. Martin, Peroxy radicals as measured in ROSE and estimated from photostationary state deviations, *J. Geophys. Res.*, *98*, 18,355-18,366, 1993.

Carroll, M. A., and A. M. Thompson, NO_x in the nonurban troposphere, in *Current Problems and Progress in Atmospheric Chemistry*, edited by J. R. Barker, pp. 199-255, World Sci., River Edge, N.J., 199-255, 1995.

Carroll, M. A., et al., Aircraft measurements of NO_x over the eastern Pacific and continental United States and implications for ozone production, *J. Geophys. Res.*, *95*, 10,205-10,233, 1990.

Carroll, M. A., et al., The local photochemical environment and ozone production and loss at Sable Island, Nova Scotia, derived from measurements made during the NARE 1993 Summer Intensive (abstract), *Eos Trans., AGU*, *75* (44), Fall Meet. Suppl., 118, 1994.

Carsey, T. P., D. D. Churchill, M. L. Farmer, C. J. Fischer, A. A. Pszenny, V. B. Ross, E. S. Saltzman, M. Springer-Young, and B. Bonsang, Nitrogen oxides and ozone production in the North Atlantic marine boundary layer, *J. Geophys. Res, 102*, 10,653-10,665, 1997.

Carter, W. P. L., A detailed mechanism for the gas-phase atmospheric reactions of organic compounds, *Atmos. Environ., Part A, 24*, 481-518, 1990.

Chameides, W. L., D.D. Davis, M. O. Rodgers, J. Bradshaw, G. Sachse, G. Hill, G. Gregory, and R. Rasmussen, Net ozone photochemical production over the eastern and central North Pacific as inferred from GTE/CITE 1 observations during fall 1983, *J. Geophys. Res., 92*, 2131-2152, 1987.

Chameides, W. L., et al., Observed and model-calculated NO_2/NO ratios in tropospheric air sampled during the NASA GTE/CITE-2 field study, *J. Geophys. Res., 95*, 10,235-10,247, 1990.

Chameides, W. L., et al., Ozone precursor relationships in the ambient atmosphere, *J. Geophys. Res., 97*, 6037-6055, 1992.

Chatfield, R. B., and A. C. Delany, Convection links biomass burning to increased tropical ozone: However, models will tend to overpredict O_3, *J. Geophys. Res., 95*, 18,473-18,488, 1990.

Daum, P. H., L. I. Kleinman, A. J. Hills, A. L. Lazrus, A. C. D. Leslie, K. Busness, and J. Boatman, Measurement and interpretation of concentrations of H_2O_2 and related species in the upper Midwest during summer, *J. Geophys. Res., 95*, 9857-9871, 1990.

Daum, P. H., L. I. Kleinman, L. Newman, W. T. Luke, J. Wienstein-Lloyd, C. M. Berkowitz, and K. M. Busness, Chemical and physical properties of plumes of anthropogenic pollutants transported over the North Atlantic during NARE, *J. Geophys. Res., 101*, 29,029-29,042, 1996.

Davis, D. D., et al., Assessment of ozone photochemistry in the western North Pacific as inferred from PEM-West A observations during the fall 1991, *J. Geophys. Res., 101*, 2111-2134, 1996a.

Davis, D., J. Crawford, S. Liu, S. McKeen, A. Bandy, D. Thornton, F. Rowland, and D. Blake, Potential impact of iodine on tropospheric levels of ozone and other critical oxidants, *J. Geophys. Res., 101*, 2135-2147, 1996b.

DeMore, W. B., S. P. Sander, D. M. Golden, M. J. Molina, R. F. Hampson, C. E. Kolb, M. J. Kurylo, C. J. Howard, and A. R. Ravishankara, Chemical kinetics and photochemical data for use in stratospheric modeling, *JPL. Publ., 92-20*, 1992.

Emmons, L. K., et al., Climatologies of NO_x and NO_y: A comparison of data and models, *Atmos. Environ., 31*, 1851-1903, 1997.

Fehsenfeld, F. C., M. Trainer, D. D. Parrish, A. Volz-Thomas, and S. Penkett, North Atlantic Regional Experiment 1993 summer intensive: Foreword, J. Geophys. Res., 101, 28,869-28,875, 1996a.

Fehsenfeld, F. C., M. Trainer, and D. D. Parrish, Transport and processing of O_3 and O_3 precursors over the North Atlantic: An overview of the 1993 North Atlantic Regional Experiment (NARE) summer intensive, J. Geophys. Res., 101, 28,877-28,891, 1996b.

Finlayson-Pitts, B. J., and J. N. Pitts, Atmospheric Chemistry, Fundamentals and Experimental Techniques, 408 pp., John Wiley, New York, 1986.

Finlayson-Pitts, B. J., F. E. Livingston, and H. N. Berko, Ozone destruction and bromine photochemistry in the Arctic spring, Nature, 343, 622-625, 1990.

Fishman, J., S. Solomon, and P. J. Crutzen, Observational and theoretical evidence in support of a significant in situ photochemical source of tropospheric ozone, Tellus, 31, 432-446, 1979.

Fishman, J., C. E. Watson, J. C. Larsen, and J. A. Logan, Distribution of tropospheric ozone determined from satellite data, J. Geophys. Res., 95, 3599-3617, 1990.

Gao, D., W. R. Stockwell, and J. B. Milford, Global uncertainty analysis of a regional-scale gas-phase chemical mechanism, J. Geophys. Res., 101, 9107-9119, 1996.

Guenther, A., et al., A global model of natural volatile organic compound emissions, J. Geophys. Res., 100, 8873-8892, 1995.

Guenther, A., P. Zimmerman, L. Klinger, J. Greenberg, C. Ennis, K. Davis, W. Pollock, H. Westberg, E. Allwine, and C. Geron, Estimates of regional natural volatile organic compound fluxes from enclosure and ambient measurements, J. Geophys. Res., 101, 1345-1359, 1996.

Hauglustaine, D. A., B. A. Ridley, S. Solomon, P. G. Hess, and S. Madronich, HNO_3/NO_x ratio in the remote troposphere during MLOPEX 2: Evidence for nitric acid reduction on carbonaceous aerosols?, Geophys. Res. Lett., 23, 2609-2612, 1996.

Heikes, B. G., et al., Hydrogen peroxide and methylhydroperoxide distributions related to ozone and odd hydrogen over the North Pacific in the fall of 1991, J. Geophys. Res., 101, 1891-1905, 1996.

Hirsh, R. M., and E. J. Gilroy, Methods of fitting a straight line to data: Examples in water resources, Water Resour. Bull., 20, 705-711, 1984.

Hough, A. M., and R. G. Derwent, Changes in the global concentration of tropospheric ozone due to human activities, Nature, 344, 645-648, 1990.

Hwang, H., and P. K. Dasgupta, Thermodynamics of the hydrogen peroxide-water system, Environ. Sci. Technol., 19, 255-258, 1985.

Intergovernmental Panel on Climate Change (IPCC), Climate Change: The Scientific Assessment, edited by J. T. Houghton, G. J. Jenkins, and J. J. Ephraums, Cambridge Univ. Press, New York, 1990.

International Global Atmospheric Chemistry (IGAC), The International Global Atmospheric Chemistry Project: An Overview, MIT Press, Cambridge, Mass., 1992.

Jacob, D. J., and S. C. Wofsy, Photochemistry of biogenic emissions over the Amazon forest, J. Geophys. Res., 93, 1477-1486, 1988.

Jacob, D. J., et al., Summertime photochemistry of the troposphere at high northern latitudes, J. Geophys. Res., 97, 16,421-16,431, 1992.

Jacob, D. J., J. A. Logan, G. M. Gardner, R. M. Yevich, C. M. Spivakovsky, S. C. Wofsy, S. Sillman, and M. J. Prather, Factors regulating ozone over the United States and its export to the global atmosphere, J. Geophys. Res., 98, 14,817-14,826, 1993.

Jacob, D. J., et al., The origin of ozone and NO_x in the tropical troposphere: A photochemical analysis of aircraft observations over the South Atlantic Basin, J. Geophys. Res., 101, 24,235-24,250, 1996.

Joffre, S. M., Modeling the dry deposition velocity of highly soluble gases to the sea surface, Atmos. Environ., 22, 1137-1146, 1988.

Kleinman, L., et al., Ozone formation at a rural site in the southeastern United States, J. Geophy. Res., 99, 3469-3482, 1994.

Kleinman, L. I., P. H. Daum, Y.-N. Lee, S. R. Springston, L. Newman, W. R. Leaitch, C. M. Banic, G. A. Isaac, and J. I. MacPherson, Measurement of O_3 and related compounds over southern Nova Scotia, 1, Vertical distribution, J. Geophys. Res., 101, 29,043-29,060, 1996.

Lacis, A. A., D. J. Wuebbles, and J. A. Logan, Radiative forcing of climate by changes in the vertical distribution of ozone, J. Geophys. Res., 95, 9971-9981, 1990.

Lamb, B., A. Guenther, D. Gay, and H. Westberg, A national inventory of biogenic hydrocarbon emissions, Atmos. Environ., 21, 1695-1705, 1987.

Lee, J. H., D. F. Leahy, I. N. Tang, and L. Newman, Measurement and speciation of gas phase peroxides in the atmosphere, J. Geophys. Res., 98, 2911-2915, 1993.

Lelieveld, J., The role of clouds in tropospheric photochemistry, Ph.D. dissertation, Utrecht Univ., Netherlands, 1990.

Lelieveld, J., and P. J. Crutzen, Influences of cloud photochemical processes on tropospheric ozone, Nature, 343, 227-233, 1990.

Levy, H., II, J. D. Mahlman, W. J. Moxim, and S. C. Liu, Tropospheric ozone: The role of transport, J. Geophys. Res., 90, 3753-3772, 1985.

Lin, X., M. Trainer, and S. C. Liu, On the nonlinearity of the tropospheric ozone production, J. Geophys. Res., 93, 15,879-15,888, 1988.

Liu, S. C., D. Kley, M. McFarland, J. D. Mahlman, and H. Levy II, On the origin of tropospheric ozone, J. Geophys. Res., 85, 7546-7552, 1980.

Liu, S. C., M. McFarland, D. Kley, O. Zafiriou, and B. Huebert, Tropospheric NO_x and O_3 budgets in the equatorial Pacific, J. Geophys. Res., 88, 1360-1368, 1983.

Liu, S. C., M. Trainer, F. C. Fehsenfeld, D. D. Parrish, E. J. Williams, D. W. Fahey, G. Hubler, and P. C. Murphy, Ozone production in the rural troposphere and the implications for regional and global ozone distributions, J. Geophys. Res., 92, 4191-4207, 1987.

Logan, J. A., Tropospheric ozone: Seasonal behavior, trends, and anthropogenic influence, J. Geophys. Res., 90, 10,463-10,482, 1985.

Logan, J. A., Ozone in rural areas of the United States, J. Geophys. Res., 94, 8511-8532, 1989.

Logan, J. A., M. J. Prather, S. C. Wofsy, and M. B. McElroy, Tropospheric chemistry: A global perspective, J. Geophys. Res., 86, 7210-7254, 1981.

Lurmann, F. W., A. C. Lloyd, and R. Atkinson, A chemical mechanism for use in long-range transport/acid deposition computer modeling, J. Geophys. Res., 91, 10,905-10,936, 1986.

Madronich, S., Photodissociation in the atmosphere, 1, Actinic flux and the effects of ground reflections and clouds, J. Geophys. Res., 92, 9740-9752, 1987a.

Madronich, S., Intercomparison of NO_2 photodissociation and U.V. radiometer measurements, Atmos. Environ., 21, 569-578, 1987b.

Marenco, A. and F. Said, Meridional and vertical ozone distribution in the background troposphere (70°N-60° S; 0-12 km altitude) from scientific aircraft measurements during

the STRATOZ III experiment (June 1984), *Atmos. Environ., 23*, 201-214, 1989.

Mauzerall, D. L., D. J. Jacob, S.-M. Fan, J. D. Bradshaw, G. L. Gregory, G. W. Sachse, and D. R. Blake, Origin of tropospheric ozone at remote high northern latitudes in summer, *J. Geophys. Res., 101*, 4175-4188, 1996.

Merrill, J. T., and J. L. Moody, Synoptic meteorology and transport during the North Atlantic Regional Experiment (NARE) intensive, *J. Geophys. Res., 101*, 28,903-28,921, 1996.

Mihelcic, D., P. Busgen, M. Schultz, A. Volz-Thomas, and R. Schmitt, Peroxy radical concentrations and the ratio of hydroperoxy to organic peroxy radicals at Izaña (Tenrife): Direct measurements by Matrix Isolation/ESR-Spectroscopy (abstract), *Eos Trans., AGU, 75* (44), Fall Meet. Suppl., 93, 1994.

Milford, J. B., D. Gao, A. G. Russell, and G. J. McRae, Use of sensitivity analysis to compare chemical mechanisms for air-quality modeling, *Environ. Sci. Technol., 26*, 1179-1189, 1992.

Moody, J. L., C. Davenport, J. T. Merrill, S. J. Oltmans, M. Trainer, M. Buhr, D. D. Parrish, J. S. Holloway, H. Levy II, and G. L. Forbes, Meteorological mechanisms for transporting ozone over the western North Atlantic Ocean: A case study for August 25-30, 1993, *J. Geophys. Res., 101*, 29,213-29,228, 1996.

Muller, J.-F. and G. Brasseur, IMAGES: A three-dimensional chemical transport model of the global troposphere, *J. Geophys. Res., 100*, 16,445-16,490, 1995.

Noone, K. J., R. D. Schillawski, G. L. Kok, C. S. Bretherton, and B. J. Huebert, Ozone in the marine atmosphere observed during the Atlantic Stratocumulus Transition Experiment/Marine Aerosol and Gas Exchange, *J. Geophys. Res., 101*, 4485-4499, 1996.

Norton, R. B., D. D. Parrish, J. S. Holloway, J. M. Roberts, F. C. Fehsenfeld, and S. Bertman, Episodes of extensive removal of PAN and HNO₃ from the marine boundary layer at Chebogue Point., Nova Scotia (abstract), *Eos Trans., AGU, 75* (44), Fall Meet. Suppl., 93, 1994.

Olson, J., et al., Results from the Intergovernmental Panel on Climatic Change Photochemical Model Intercomparison (PhotoComp), *J. Geophys. Res., 102*, 5979-5991, 1997.

Oltmans, S. J., and H. Levy II, Surface ozone measurements from a global network, *Atmos. Environ., 28*, 9-24, 1994.

Parrish, D. D., M. Trainer, E. J. Williams, D. W. Fahey, G. Hubler, C. S. Eubank, S. C. Liu, P. C. Murphy, D. L. Albritton, and F. C. Fehsenfeld, Measurements of the NOₓ-O₃ photostationary state at Niwot Ridge, Colorado, *J. Geophys. Res., 91*, 5361-5370, 1986.

Parrish, D. D., J. S. Holloway, M. Trainer, P. C. Murphy, G. L. Forbes, and F. C. Fehsenfeld, Export of North American ozone pollution to the North Atlantic Ocean, *Science, 259*, 1436-1439, 1993.

Parrish, D.D., J. S. Holloway, and F. C. Fehsenfeld, Routine continous measurements of carbon monoxide with parts per billion precision, *Environ. Sci. Technol., 28*, 1615-1618, 1994.

Parrish, D.D., M. Trainer, J. S. Holloway, J. E. Yee, M. S. Warshawsky, F. C. Fehsenfeld, G. Forbes, and J. L Moody, Relationships between ozone and carbon monoxide at surface sites in the North Atlantic Region, *J. Geophys. Res.*, this issue.

Ridley, B. A., S. Madronich, R. B. Chatfield, J. G. Walega, R. E. Shetter, M. A. Carroll, and D. D. Montzka, Measurements and model simulations of the photostationary state during the Mauna Loa Observatory Photochemistry Experiment: Implications for radical concentrations and ozone production and loss rates, *J. Geophys. Res., 97*, 10,375-10,388, 1992.

Roberts, J. M., et al., Removal of NO_y species from the marine boundary layer over the North Atlantic, *J. Geophys. Res., 101*, 28,947-28,968, 1996.

Schwartz, S. E., and W. H. White, Solubility equilibria of the nitrogen oxides and oxyacids in dilute aqueous solution, *Adv. Environ. Sci. Eng., 4*, 1, 1981.

Seinfeld, J. H., *Atmospheric Chemistry and Physics of Air Pollution*, p.8, John Wiley, New York, 1986.

Sillman, S., J. A. Logan, and S. C. Wofsy, The sensitivity of ozone to nitrogen oxides and hydrocarbons in regional ozone episodes, *J. Geophys. Res., 95*, 1837-1851, 1990a.

Sillman, S., J. A. Logan, and S. C. Wofsy, A regional scale model for ozone in the United States with subgrid representation of urban and power plant plumes, *J. Geophys. Res., 95*, 5731-5748, 1990b.

Sillman, S., P. J. Samson, and J. M. Masters, Ozone production in urban plumes transported over water: Photochemical model and case studies in the northeastern and Midwestern United States, *J. Geophys. Res., 98*, 12,687-12,699, 1993.

Singh, H. B., G. L. Gregory, B. Anderson, E. Browell, G. W. Sachse, D. D. Davis, J. Crawford, J. D. Bradshaw, R. Talbot, D. R. Blake, D. Thornton, R. Newell, and J. Merrill, Low ozone in the marine boundary layer of the tropical Pacific Ocean: Photochemical loss, chlorine atoms, and entrainment, *J. Geophys. Res., 101*, 1907-1918, 1996.

Stockwell, W. R., On the HO₂ + HO₂ reaction: Its misapplication in atmospheric chemistry models, *J. Geophys. Res., 100*, 11,695-11,698, 1995.

Thompson, A. M., The oxidizing capacity of the Earth's atmosphere: Probable past and future changes, *Science, 256*, 1157-1165, 1992.

Thompson, A. M., and O. C. Zafiriou, Air-sea fluxes of transient atmospheric species, *J. Geophys. Res., 88*, 6696-6708, 1983.

Trainer, M., E. Y. Hsie, S. A. McKeen, R. Tallamraju, D. D. Parrish, F. C. Fehsenfeld, and S. C. Liu, Impact of natural hydrocarbons on hydroxyl and peroxy radicals at a remote site, *J. Geophys. Res., 92*, 11,879-11,894, 1987.

Trainer, M., et al., Observations and modeling of the reactive nitrogen photochemistry at a rural site, *J. Geophys. Res., 96*, 3045-3063, 1991.

Trainer, M., et al., Correlation of ozone with NO_y in photochemically aged air, *J. Geophys. Res., 98*, 2917-2925, 1993.

U.S. Environmental Protection Agency (EPA), Review of the National Ambient Air Quality Standards for ozone, Assessment of scientific and technical information, draft staff paper, Air Qual. Manage. Div., Off. of Air Qual. Plann. and Stand., Research Triangle Park, N. C., 1988.

Voldner, E. C., L. A. Barrie, and A. Sirois, A literature review of dry deposition of oxides of sulphur and nitrogen with emphasis on long-range transport modeling in North America, *Atmos. Environ., 20*, 2101-2123, 1986.

Volz, A., and D. Kley, Evaluation of the Montsouris series of ozone measurements made in the nineteenth century, *Nature, 332*, 240-242, 1988a.

Volz, A., D. Mihelcic, P. Musgen, H. W. Patz, G. Pilwat, H. Geiss, and D. Kley, Ozone production in the Black Forest: Direct measurements of RO₂, NOₓ and other relevant parameters, in *Tropospheric Ozone: Regional and Global Scale Interactions*, edited by I. S. A. Isaksen, pp. 293-302, D. Reidel, Norwell, Mass., 1988b.

Wang, T., et al., Ground-based measurements of NOₓ and total reactive oxidized nitrogen NO_y at Sable Island, Nova Scotia, during the NARE 1993 summer intensive, *J. Geophys. Res., 101*, 28,991-29,004, 1996.

Wendland, W. M., and R. A. Bryson, Northern hemisphere airstream regions, *Mon. Weather Rev., 109*, 255-270, 1981.

Wild, O., K. S. Law, D. S. MacKenna, B. J. Bandy, S. A. Penkett, and J. A. Pyle, Photochemical trajectory modeling studies of the North Altantic region during August 1993, *J. Geophys. Res.*, *101*, 29,269-29,288, 1996.

Yang, Y., W. R. Stockwell, and J. B. Milford, Uncertainties in incremental reactivities of volatile organic compounds, *Environ. Sci. Technol.*, *29*, 1336-1345, 1995.

G. M. Albercook, M. A. Carroll, K. A. Duderstadt, L. Feng, and S. Sillman, Department of Atmospheric, Oceanic, and Space Sciences, University of Michigan, Ann Arbor, MI 48109. (e-mail: mcarroll@umich.edu; kathyd@engin.umich.edu; sillman@kudzu.sprl.umich.edu)

D. R. Blake and N. J. Blake, Department of Chemistry, University of California at Irvine, Irvine, CA 92717.

F. C. Fehsenfeld, J. S. Holloway, and D. D. Parrish, Aeronomy Laboratory, National Oceanic and Atmospheric Administration, Boulder, CO 80303.

G. Forbes, Atmospheric Environment Service, Sable Island, Nova Scotia, Canada.

T. Wang, Environmental Engineering Unit, Department of Civil and Structural Engineering, Hong Kong Polytechnic University, Hung Hom, Kowloon, Hong Kong.